Manifestation and consequences of warming and altered heat fluxes over the Bering and Chukchi Sea continental shelves

S.L. Danielson [a],[*], O. Ahkinga [b], C. Ashjian [c], E. Basyuk [d], L.W. Cooper [e], L. Eisner [f], E. Farley [g], K. B. Iken [a], J.M. Grebmeier [e], L. Juranek [h], G. Khen [d], S.R. Jayne [c], T. Kikuchi [i], C. Ladd [j], K. Lu [a], R. M. McCabe [k], G.W.K. Moore [l], S. Nishino [i], F. Ozenna [b], R.S. Pickart [c], I. Polyakov [m,p], P. J. Stabeno [j], R. Thoman [n], W.J. Williams [o], K. Wood [k], T.J. Weingartner [a]

[a] University of Alaska Fairbanks (UAF), College of Fisheries and Ocean Sciences, Fairbanks, AK, USA
[b] Native Village of Diomede, Diomede, AK, USA
[c] Woods Hole Oceanographic Institute, Woods Hole, MA, USA
[d] Russian Federal Research Institute of Fisheries and Oceanography, Pacific Branch of VINRO, TINRO, Vladivostok, Russia
[e] University of Maryland Center for Environmental Sciences, Chesapeake Biological Laboratory, Solomons, MD, USA
[f] National Oceanographic and Atmospheric Administration, Alaska Fisheries Science Center, Seattle, WA, USA
[g] NOAA, Alaska Fisheries Science Center, Ted Stevens Marine Research Institute, Juneau, AK, USA
[h] College of Earth, Ocean and Atmospheric Science, Oregon State University, Corvallis, OR, USA
[i] Institute of Arctic Climate and Environment Research (IACE), Research Institute for Global Change (RIGC), Japan Agency for Marine-Earth Science and Technology (JAMSTEC), Yokosuka, Kanagawa, Japan
[j] National Oceanographic and Atmospheric Administration (NOAA), Pacific Marine Environmental Laboratory, Seattle, WA, USA
[k] University of Washington, Joint Institute for the Study of the Atmosphere and Ocean, Seattle, WA, USA
[l] University of Toronto Mississauga, Mississauga, ON, Canada
[m] UAF International Arctic Research Center and College of Natural Science and Mathematics, 930 Koyukuk Drive, Fairbanks, AK, 99775, USA
[n] UAF, Alaska Center for Climate Assessment and Policy, Fairbanks, AK, USA
[o] Institute of Ocean Sciences, Fisheries and Oceans Canada, Sidney, BC, Canada
[p] Finnish Meteorological Institute, Erik Palménin aukio 1, 00560, Helsinki, Finland

ARTICLE INFO

ABSTRACT

A temperature and salinity hydrographic profile climatology is assembled, evaluated for data quality, and analyzed to assess changes of the Bering and Chukchi Sea continental shelves over seasonal to century-long time scales. The climatology informs description of the spatial distribution and temporal evolution of water masses over the two shelves, and quantification of changes in the magnitude and throughput of heat and fresh water. For the Chukchi Shelf, linear trend analysis of the integrated shelf heat content over its 1922–2018 period of record finds a significant summer and fall warming of 1.4 °C (0.14 ± 0.07 °C decade^{-1}); over 1990–2018 the warming rate tripled to 0.43 ± 0.35 °C decade^{-1}. In contrast, the Bering Shelf's predominantly decadal-scale variability precludes detection of a water column warming trend over its 1966–2018 period of record, but sea surface temperature data show a significant warming of 0.22 ± 0.10 °C decade^{-1} over the same time frame. Heat fluxes over 1979–2018 computed by the European Centre for Medium-Range Weather Forecast (ECMWF) ERA5 reanalysis exhibit no record-length trend in the shelf-wide Bering surface heat fluxes, but the Chukchi Shelf cooling season (October–March) has a trend toward greater surface heat losses and its warming season (April–September) has a trend toward greater heat gains. The 2014–2018 half-decade exhibited unprecedented low winter and spring sea-ice cover in the Northern Bering and Chukchi seas, changes that coincided with reduced springtime surface albedo, increased spring absorption of solar radiation, and anomalously elevated water column heat content in summer and fall. Consequently, the warm ocean required additional time to cool to the freezing point in fall. Fall and winter ocean-to-atmosphere heat fluxes were anomalously large and associated with enhanced southerly winds and elevated surface air temperatures, which in turn promoted still lower sea-ice production, extent, and concentration anomalies. Likely reductions in sea-ice melt were associated with positive salinity anomalies on the Southeast Bering Shelf and along the continental slope over 2014–2018. Negative

* Corresponding author.
  E-mail address: sldanielson@alaska.edu (S.L. Danielson).

salinity anomalies during 2014–2018 on the central and northern Bering Shelf may be related to a combination of 1) long-term declines in salinity, 2) an increase of ice melt, and 3) a decline of brine production. We hypothesize that freshening on the Bering Shelf and in Bering Strait since 2000 are linked to net glacial ablation in the Gulf of Alaska watershed. We show that the heat engines of both the Bering and Chukchi shelves accelerated over 2014–2018, with increased surface heat flux exchanges and increased oceanic heat advection. During this time, the Chukchi Shelf delivered an additional 5–9 x 10^{19} J yr^{-1} (50–90 EJ yr^{-1}) into the Arctic basin and/or sea-ice melt, relative to the climatology. A similar amount of excess heat (60 EJ yr^{-1}) was delivered to the atmosphere, showing that the Chukchi Sea makes an out-sized contribution to Arctic amplification. A conceptual model that summarizes the controlling feedback loop for these Pacific Arctic changes relates heat content, sea ice, freshwater distributions, surface heat fluxes, and advective fluxes.

1. Introduction

Oceanic and atmospheric transport of heat from low to high latitudes contributes to global thermal regulation (Trenberth et al., 2009), but greenhouse warming regionally perturbs heat content and fluxes (Stocker et al., 2013), causing the earth's climate system and biological systems to adjust in response. These adjustments include alterations to sea ice (Stroeve et al., 2005; Perovich et al., 2008), permafrost (Osterkamp and Romanovsky, 1999), precipitation (Groves and Francis, 2002), and many components of both terrestrial and marine ecosystems (Walther et al., 2002; Doney et al., 2011). At high latitudes in the Northern Hemisphere, reinforcing feedback loops induce faster rates of atmospheric warming than elsewhere, resulting in the "Arctic amplification" of global climate warming (Serreze and Francis, 2006; Hansen
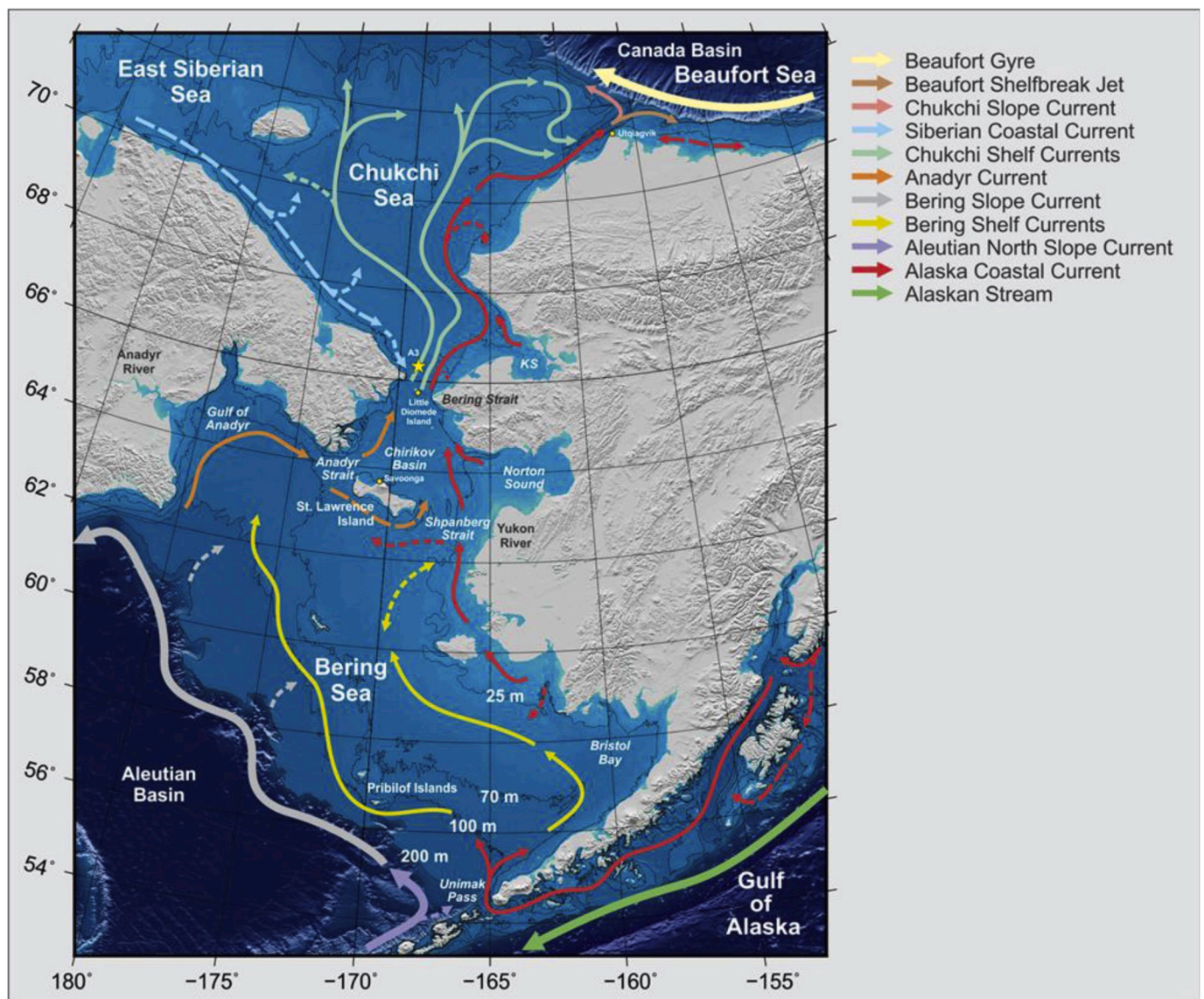
Fig. 1. Location map of the Pacific Arctic region with water body and place names. Persistent currents are shown with solid arrows; intermittent or poorly known flows are denoted with dashed arrows. Bering Strait mooring A3 is marked with a yellow star. Abbreviation KS denotes Kotzebue Sound. Depth isopleths are contoured with thin black lines at 25, 70, 100 and 200 m. (For interpretation of the references to color in this figure legend, the reader is referred to the Web version of this article.)

et al., 2010; Overland and Wang, 2010; Screen and Simmonds, 2010; Serreze and Barry, 2011). In this study, we quantify recent (years) and long-term (decades to century) changes in shelf temperatures, salinities, and air-sea heat exchanges over the Bering and Chukchi continental shelves (Fig. 1), examining the local manifestation and consequences of Arctic amplification within the context of the prior period of record.

Marine ecosystems of the Bering-Chukchi shelves encompass economically important fishing grounds (Van Vorhees and Lowther, 2010), productive benthos (Grebmeier et al., 2015), and subsistence resources for Indigenous coastal communities (Suydam et al., 2006), all of which derive fundamental structure from the regional environmental conditions (Hare and Mantua, 2000; Benson and Trites, 2002; Hunt et al., 2011). For example, oceanic heat content (Walsh et al., 2018) is important to sea-ice extent and duration (Woodgate et al., 2010; Frey et al., 2015; Danielson et al., 2017; Polyakov et al., 2017), which in turn affect trophic exchanges (Coyle et al., 2011), prevalence of harmful algal blooms (Natsuike et al., 2017), and species distributions (Mueter and Litzow, 2008). Temperature is by itself an important control on growth rates (Eppley, 1972) and oxygen respiration (Ikeda, 1985, 2001). A better understanding of ongoing and past environmental change is a first step to exploring how bottom-up forcing may propagate through the Arctic ecosystem in the future.

In the 2013/2014 winter, the North Pacific experienced surface and subsurface warming that resulted from a persistent atmospheric blocking ridge located over western North America (Bond et al., 2015) and meridional modes of atmospheric teleconnections that directed heat away from the tropics (Di Lorenzo and Mantua, 2016). This was followed by a strong 2015 El Niño (McPhaden, 2015) and additional atmospheric blocking patterns that extended the marine heat wave. The Bering Sea also experienced previously undocumented and unprecedented high sea surface temperatures in 2014 (Stabeno et al., 2017), which by sea surface temperature (SST) and heat content metrics have

continued to persist into 2018 (Thoman et al., 2020) and 2019 (Cornwall, 2019; Stabeno and Bell, 2019). The upper ocean heat content (0–300 m integration) for the eastern Bering Sea exhibited warm anomalies that were correlated with SST variations (Walsh et al., 2018). The recent warm anomalies are superimposed upon longer term warming trends previously identified for the Bering and Chukchi seas (Steele et al., 2008; Woodgate et al., 2010; Woodgate et al., 2012; Tokinaga et al., 2017).

Recent weather patterns and sea ice conditions in the northern Bering and southern Chukchi seas are challenging long-held understanding of what constitutes winter norms. The two Diomede Islands, in the past connected by shorefast ice through the winter months (sufficient to support commercial airline service on an ice runway), were exposed in January and February 2018 to long fetch open water and unconsolidated sea ice that allowed massive waves to roll ashore in a late February 2018 storm (Fig. 2). Mid-winter conditions of 2019 brought similarly low sea-ice extents to the region (Cornwall, 2019). These unprecedented observations are illustrative of conditions at the epicenter of Arctic amplification over the Pacific sector: sea ice loss over the Bering-Chukchi shelves.

The broad eastern Bering and Chukchi Sea continental shelves, connected by the narrow (~85 km) Bering Strait, comprise the shallow expanse (average < 70 m) across which Pacific waters carrying heat, fresh water and nutrients are transported into the Arctic (Coachman and Aagaard, 1966; Stigebrandt, 1984; Walsh et al., 1989). Based on oceanographic mooring data, the annual mean volume flux northward through Bering Strait is thought to be approximately 1 Sv (1 Sv = 10^6 m^3 s^{-1}) (Woodgate, 2018), having increased to this level from roughly 0.8 Sv in the 1990s and early 2000s (Roach et al., 1995; Woodgate et al., 2005a, 2015; Woodgate, 2018). The increasing volume transport (~0.2 Sv decade^{-1}) and a weakly increasing trend in the observed temperature (0.27 ± 0.23 °C decade^{-1}) both contribute to an increasing trend in the
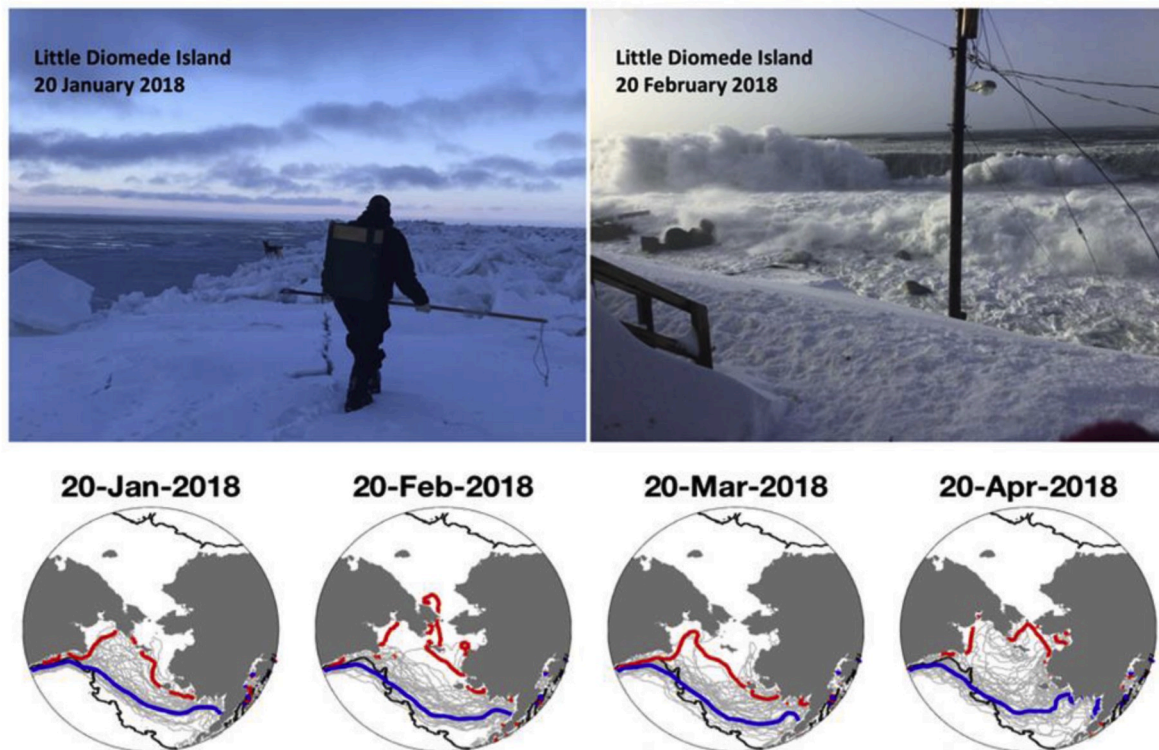
Fig. 2. Open water seen in late January (top left) and February (top right) 2018 from Little Diomede Island, which was historically located far north of the ice edge at this time of year. Satellite-derived ice edge locations (bottom) show the 1979–2018 climatological (blue) and 2018 (red) 15% concentration contours for the 20th of January, February, March, and April. Corresponding ice edges for all years over 1979–2017 are shown with gray contours. The 200 m isobath (black contour) shows the shelf break location. Photographs by O. Ahkinga (left) and F. Ozenna (right). (For interpretation of the references to color in this figure legend, the reader is referred to the Web version of this article.)

northward heat flux (Woodgate, 2018). Measurements also document a modest freshening of ~0.14±0.10 decade^{-1} over 1991–2015 that together with the increasing transport have increased the Pacific origin freshwater flux into the Arctic by ~40% or more (Woodgate, 2018). It is worth noting that the Bering Strait throughflow is the only oceanic inflow to the Arctic showing significant change in volume transport over 1993–2015 but the trend magnitude in Bering Strait is smaller than the trend uncertainty of other inflow pathways (Østerhus et al., 2019), leaving the system-wide balance unclear. In the absence of wind forcing, vorticity constraints confine much of the Bering Strait inflow to an advective pathway that circumscribes the Gulf of Anadyr in a clockwise fashion and enters the Bering Strait region via Anadyr Strait (Kinder et al., 1986), leaving the bulk of the eastern Bering Sea shelf as a secondary feed to the Bering Strait throughflow via Shpanberg Strait, east of St. Lawrence Island (Danielson et al., 2012a). Variations in these currents can alter Pacific-Arctic exchanges and the seasonal evolution of sea ice and water properties.

Processes that perturb the mean circulation and spatial distributions of water properties vary temporally and regionally across these shelves. For example, on interannual and longer time scales, variations in the Bering Strait throughflow have been ascribed to a combination of local wind stress (Aagaard et al., 1985; Woodgate et al., 2012; Danielson et al., 2014; Woodgate, 2018), wind stress over the adjoining basin and adjoining shelves (Danielson et al., 2014), variability in regional pressure gradients, especially in relation to the western Chukchi and East Siberian Sea (Danielson et al., 2014; Peralta-Ferriz and Woodgate, 2017; Okkonen et al., 2019), and thermohaline variations (Aagaard et al., 2006). Regional wind and buoyancy forces drive the seasonally warm Alaskan Coastal Current (ACC) (Paquette and Bourke, 1974; Ahlnäs and Garrison, 1984; Gawarkiewicz et al., 1994; Wiseman and Rouse, 1980; Woodgate and Aagaard, 2005) and the cool but fresh Siberian Coastal Current (Weingartner et al., 1999), which is present only in some years in the Chukchi Sea. Both coastal currents are near-shore and low-salinity features of the high latitude riverine coastal domain continuum (Carmack et al., 2015). Baroclinically unstable fronts separating ice-melt plumes from denser and warmer shelf waters (Lu et al., 2015) may be important to ocean-ice-atmosphere feedbacks and the seasonal melt-back of the Chukchi sea ice. Energetic eddies in the Bering Slope Current (Ladd, 2014), tidal energy fluxes (Foreman et al., 2006) and wind-driven exchanges, especially upwelling within shelfbreak canyons (Bourke and Paquette, 1976; Woodgate et al., 2005b; Danielson et al., 2012b) may impact cross-slope exchanges.

Although all consequences of thermal, haline, and advective variations over the Bering and Chukchi shelves are not well understood, under a warming climate it is reasonable to anticipate altered lateral and vertical property gradients that in turn will impact local and downstream habitats and potentially feed-back on the processes mentioned above. The Bering Shelf is downstream of heat and fresh water on the Gulf of Alaska shelf via Unimak Pass (Weingartner et al., 2005a). The Canada Basin is downstream of the Chukchi Shelf, which, in turn, is downstream of the Bering Sea via Bering Strait. The flows connecting these two shelves do not drain all parts of the Bering Sea shelf equally (e. g. Danielson et al., 2012a, 2012b), nor are all parts of the Chukchi uniformly flushed (e.g. Weingartner et al., 2005b; Woodgate et al., 2005c; Lin et al., 2019). The fate of Pacific-origin heat and fresh water is important to the Arctic Ocean's thermohaline structure (Aagaard et al., 1981; Shimada et al., 2005; Woodgate et al., 2012; Timmermans et al., 2014, 2018); the thickness of sea ice (Kwok and Untersteiner, 2011) and the timing with which it forms and melts (Steele et al., 2008; Jackson et al., 2012; Woodgate et al., 2010; Serreze et al., 2016); and the Arctic atmospheric heat budget (Serreze et al., 2007). Ice-related processes are critically dependent on the local heat balance so alterations to advective heat fluxes carry the potential for profoundly reorganizing the ecosystem. Given these roles for the Bering Strait throughflow in relation to a changing Arctic, an important goal for this paper is to develop an improved understanding of long-term changes in the Bering and

Chukchi Seas' heat and freshwater budgets.

For the present study, we compiled temperature and salinity hydrographic profiles for the Bering and Chukchi shelves from 1922 to 2018, from which we estimate changes in heat content and freshwater content. Atmospheric reanalysis model outputs from the European Centre for Medium-Range Weather Forecast (ECMWF) ERA5 model (Copernicus Climate Change Service (C3S), 2017) provide estimates of surface heat fluxes from 1979 to 2018, and we use oceanographic mooring data from Bering Strait (Woodgate, 2018) from 1990 to 2016 to constrain oceanic advective heat fluxes from the Bering Shelf into the Chukchi Sea. Gridded surface air temperature (SAT) (Lenssen et al., 2019) and sea surface temperature (SST) (Huang et al., 2017) datasets give alternate multi-decadal perspectives of thermal conditions.

2. Data and methods

2.1. Geography

The soundings-based Alaska Region Digital Elevation Model (ARDEM; Danielson et al., 2015) provides seafloor depths on a ~1 km grid across the Bering and Chukchi shelves (Fig. 1). Using the ARDEM grid and ETOPO1 (Eakins and Sharman, 2010) digital elevation model results, we compile geographic statistics (Table 1) that summarize our primary domains of interest and are used to scale area-averaged surface fluxes, heat content, and freshwater anomaly estimates. The ARDEM depth estimates are also used to help validate hydrographic profiles and form full water column estimates of fresh water and heat contents.

2.2. Hydrography

The archive of water column profile data covering the largest number of years (first samples taken in 1922 in the Chukchi Sea and in 1966 in the Bering Sea) and providing the largest number of conductivity-temperature-depth (CTD), bottle and profiling float soundings is the National Centers for Environmental Information (NCEI) World Ocean Database 2018 (WOD18) (Boyer et al., 2018). Additional profiles come from US oceanographic expeditions in recent years for which the hydrographic data are not yet incorporated into WOD18, and archives from non-US institutions. These include data from the US National Oceanographic and Atmospheric Administration (NOAA) Pacific Marine Environmental Laboratory (PMEL) and NOAA Alaska Fisheries Science Center (AFSC) hydrographic databases, the University of Alaska Fairbanks Institute of Marine Science (UAF IMS) hydrographic database, and CTD data compiled by the Synthesis for Arctic Ocean Research (Moore et al., 2018). Additional data come from archives at the Russian Federal Research Institute of Fisheries and Oceanography (TINRO), the Fisheries and Oceans Canada's Institute of Ocean Sciences (IOS) and the Japan Agency for Marine-Earth Science and Technology (JAMSTEC). Temporal and spatial coverage of these data are shown in Fig. 3.

A data reduction scheme was implemented to minimize platform-associated bias and maximize consistency in handling profiles collected by discrete bottle casts, shipboard CTDs, tow-yo CTD systems, and autonomous float and glider profilers. Only profile data from the Chukchi and eastern Bering continental shelves were used, confined to stations located in less than 200 m water depth. Data locations were screened for position and depth errors, and data from stations with

Table 1
Regional depth, area, and volume statistics for the Eastern Bering Sea shelf (i.e. the shelf region shown in Fig. 1) and the Chukchi Sea continental shelf. Shelves are defined here as the region with depths less than 200 m.

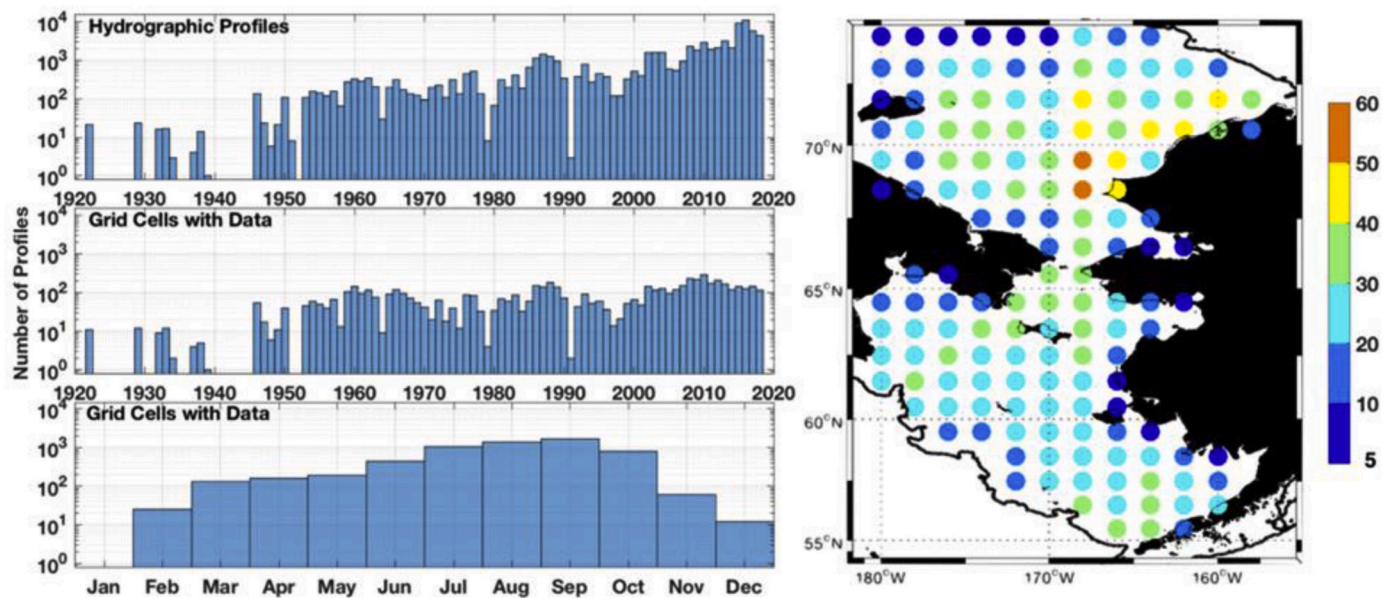|	Average Depth (m)	Surface Area (km^2)	Volume (km^3)
Arctic Ocean	1205	15,558,000	18,750,000
Chukchi Shelf	57	553,842	31,478
Bering Shelf	66	915,385	60,423

Fig. 3. Temporal and spatial coverage of gridded hydrographic profile data. The map shows the number of years represented within each grid cell. Thick black contours denote the 200 m isobath.

coordinates on land were presumed to have erroneous positions and discarded. Station data having measurements deeper than 140% of the local ARDEM bottom depth were discarded, again signaling a possible location error (errors in the ARDEM grid could also lead to spurious data discards especially in regions of steep bottom slopes). Rejecting partial profiles, we required that measurements extend at least 75% of way to the seafloor from the surface. Casts were also discarded if their shallowest measurements were from deeper than 10 m depth. Temperature data were constrained to a range of −2 to +25 °C and salinities to a range of 0–38. Any station having salinity of less than 20 at 75 m depth or deeper was assumed to be spurious and was discarded. We computed the freezing point for all data and removed casts showing data that were supercooled by more than 0.1 °C (suggesting problems with sensor calibration). Data profiles that included vertical density gradient inversions greater than 0.5 kg m^{-4} were also discarded. Following this initial screening and identification of usable profiles, we then linearly interpolated all profiles to 1 m depth intervals, extrapolated data from the deepest measurement depth to the shallower of the seafloor or 200 m, and extrapolated data from the shallowest measurement depth to the surface. Throughout, we employ the Practical Salinity Scale, using the dimensionless practical salinity units (PSU) for reporting all salinities.

The resulting data screened as described above were then gridded monthly from 1922 to 2018 on a 1° latitude by 2° longitude grid spanning 55 °N to 74 °N and 179 °E to 152 °W. Grid cells on the shelf containing fewer than 5 years of data were excluded from the climatology and analysis. In total, we reduced 69,224 hydrographic profiles into 6235 gridded profiles for an average of about 11 data points per resolved grid cell. Approximately 1600, 4500, and 27,000 of the profiles were taken from profiling floats, discrete bottles, and gliders, respectively.

At each grid cell, we evaluated the mean monthly temperature, heat content, salinity and density for the near-surface (0–10 m) layer, and for the near-bottom layer (within 10 m of the shallower of the bottom or 200 m depth). Following Woodgate et al. (2006) and others, we selected −1.9 °C (approximately the freezing point of Pacific Arctic waters) as a reference for heat content computations. Stratification was assessed by differencing water density between the near-bottom and near-surface levels. Recognizing a strong bias toward open water (summer) data collections, we generated monthly and seasonal climatological averages with winter, spring, summer and fall means created by combining data

from January to March, April to June, July to September and October to December, respectively.

2.3. Moorings

Mooring data from the Bering Strait climate monitoring mooring A3 (Woodgate, 2018) have been shown to give a useful measure of the mean water properties of the flow through the Bering Strait. This site (66.7 °N, 171.5 °W) is located ~100 km north of the Diomede Islands. The instruments record hourly temperature, salinity and velocity approximately 15 m above the bottom. From these data, estimates of volume, heat flux and freshwater flux are calculated (Woodgate, 2018). As sensors are located near the seafloor, alone these measurements underestimate heat and freshwater fluxes. Thus, simple corrections are made based either on sea surface temperature data or climatological estimates of stratification to include the effects of the seasonally present warmer surface layer and the Alaskan Coastal Current (Woodgate, 2018). The Bering Strait mooring period of record begins in 1990, missing many known cooler years during the 1970s (e.g. Overland et al., 2012). Mooring data from more recent extremely warm years from mid-2016 through 2018 are not available yet. For this reason, our initial heat budget estimates using the Bering Strait mooring data provide lower bound estimates of changes to the shelf heat budgets.

2.4. Gridded surface temperatures

For another perspective on temperature changes through time, we use the reconstructed sea surface temperature (ERSST) (Huang et al., 2017) version 5 and the NASA Surface Temperature Analysis (GISTEMP) version 4 (Lenssen et al., 2019) datasets. These compilations also provide an opportunity to examine changes over the Bering and Chukchi shelves relative to changes over larger spatial domains. The ERSST is a coarsely gridded (2° × 2°) global monthly mean SST dataset that combines historical and recent ocean surface temperature records. GISTEMP is a globally and monthly gridded dataset that provides estimates of land and ocean surface temperatures (using ERSST v5 over the ocean) based on other compilations of historical and recent weather and ocean platform data. Both datasets extend to the mid-1800s; we restrict our examinations to 1900–2018. Missing data in each compilation are replaced using statistical methods; in high latitudes records of sea-ice cover help

constrain SST estimates (Huang et al., 2017). Many early ERSST observations are based on ships logs. In the Bering and Chukchi seas, sea ice and temperature observations were commonly made from 19th and early 20th century whaling ships and patrol vessels such as those of the U.S. Revenue Cutter Service (Freeman et al., 2017).

We average the ERSST and GISTEMP data over four integration domains: the whole globe, the Arctic (latitudes $\geq$ 66 °N), the Chukchi Sea (66 °N $\leq$ latitudes $\leq$ 74 °N, 180 $\leq$ longitudes $\leq$ 156 °W), and the eastern Bering Sea (55 °N $\leq$ latitudes $\leq$ 66 °N, 180 $\leq$ longitude $\leq$ 160 °W). Selecting a reference baseline common to the profile data coverage on both shelves, we compute annual anomalies relative to the half-century covering 1966–2016.

2.5. Surface heat fluxes

We use the ECMWF ERA5 (Copernicus Climate Change Service (C3S), 2017) dataset to assess surface heat fluxes and provide supporting wind, ice cover, and air temperature data. ERA5 is a recent version release and due to higher spatial resolution, a better data assimilation scheme, and other improvements (Haiden et al., 2017), we anticipate accuracy and precision improvements relative to the prior version, ERA-Interim (Dee et al., 2011). We are unaware of an Arctic-focused assessment of ERA5 performance but evaluation of seven reanalysis products in the Arctic found that ERA-Interim was one of the three best performing reanalyses, with this product consistently scoring well for surface precipitation, shortwave and longwave fluxes, bias of air temperature at 2 m above the surface, and both temperature and wind speed correlations (Lindsay et al., 2014). Seasonally, bias in individual heat flux terms can be as large as 20–40 W m^{-2} but in aggregate the net heat flux bias was found to be < 2 W m^{-2} relative to the Lindsay et al. (2014) analyzed models' median. Many of the heat flux analyses in our study are based on differencing seasonal means that are aggregated across multiple years. For such analyses, the differencing procedure removes much of the stationary bias and we think that the resulting anomalies primarily reflect alterations in the heat exchange balance rather than nonstationary bias.

The net surface heat flux (Q_N) is computed as $Q_N = Q_{SW} + Q_{LW} + Q_{LH} + Q_{SH}$. Terms include the net shortwave (Q_{SW}), net longwave (Q_{LW}), latent (Q_{LH}) and sensible (Q_{SH}) fluxes. Because our main focus is the ocean, we assign a sign convention such that positive heat fluxes represent oceanic heat gain and negative fluxes denote oceanic heat loss.

2.6. Computation of anomalies and trends

Our results are not very sensitive to the differing climatological base periods amongst the various datasets because alternate options for multi-decade baselines of the hydrography appear more similar to each other than to the mean conditions observed over the 2014–2018 period. An advantage of including extra decades (prior to the start of the ERA5 integration or the Bering Strait mooring record) within the hydrographic baseline is that it facilitates building a more robust hydrographic climatology to help ameliorate sparse data limitations.

We compute time series anomalies relative to long-term means to facilitate unbiased assessments of change across space or time where different data subsets have differing means or variances. At each grid cell these include monthly anomalies $X^{'} = X - \overline{X_j}\big|_{j=1}^{j=12}$ where the long term (climatological) monthly mean $\overline{X_j}$ for each month ($j \in [1 \ldots 12]$) is subtracted from the monthly mean parameter X to create monthly anomaly X' time series with mean zero. The monthly standard anomaly computation $X_j^{''} = (X - \overline{X_j})/\sigma_j\big|_{j=1}^{j=12}$ normalizes each monthly anomaly by its corresponding monthly standard deviation σ, creating a time series with zero mean and unity variance. Anomalies retain units of parameter X and standard anomalies are non-dimensional.

Temporal trend analyses are based on linear regression of anomalies

and standard anomalies versus year of observation, with error estimates representing the 95% confidence interval. Statistical significance of trends that are statistically distinguishable from zero is ascribed for p-values < 0.05.

3. Results

Below, we describe the mean thermohaline structure over the two shelves and quantify changes in heat and freshwater contents over seasons and interannually. This is followed by assessment of surface heat fluxes, and finally heat budgets for the two shelves. To assess changes since the onset of the recent North Pacific marine heat wave (Bond et al., 2015), the half-decade of 2014–2018 is compared to the period of record prior to 2014.

3.1. Hydrography: climatology

We begin with temperature and salinity data, constructing a coarsely gridded seasonal climatology of the vertical profiles (Figs. S1 and S2) using water mass definitions (Table 2) that apply to both shelves and all four seasons (Fig. 4). The gridding and averaging operations smooth out spatial and temporal extremes and numerous small-scale features but nevertheless capture much of the basic hydrographic structure and its seasonal evolution, depicted with maps of water mass distributions (Fig. 5). Examinations of water masses on the Bering and Chukchi shelves typically take one of two approaches to classification. Either they follow the standard nomenclature provided by Coachman et al. (1975) describing Anadyr Water (AnW), Bering Sea Water (BSW) and Alaskan Coastal Water (ACW), or they develop an alternate classification, often necessitated by the large swing in salinities from one year to the next, that is more closely tuned to a particular dataset compilation or thermal/haline processes under consideration (e.g. Pisareva et al., 2015; Gong and Pickart, 2016; Danielson et al., 2017; Lin et al., 2019; Pickart et al., 2019). In this manuscript we develop a minimal set of classifications that can be applied across both shelves and in all seasons (but again the classification resolution lacks ability to distinguish many water mass sub-classes). We deviate from the Coachman et al. (1975) water mass designations because for the large shelf regions under consideration and our multi-season perspective the classifications BSW and ACW do not describe all water mass residence locations or natal formation regions. For example, fresh waters of the riverine coastal domain may well be termed ACW along the Alaskan coast but not in the Gulf of Anadyr. We distinguish between warm Coastal Water (wCW) and cool Coastal Water (cCW) because properties in the coastal domain vary greatly over the course of the year and alternately reflect the impact of runoff, heating, cooling, melting and freezing processes. Similarly, our warm Shelf Water

Table 2
Water mass definitions (see also Fig. 4 and the color scheme in Fig. 5).

Water Mass	Abbreviations	Temperature Range	Salinity Range
Anadyr Water	AnW	0 < T < 3	32.5 < S < 33.8
Ice Melt Water & cool Coastal Water	IMW cCW	−2 < T < 3	22 < S < 30.8
cool Shelf Water	cSW	0 < T < 3	30.8 < S < 32.5
warm Coastal Water	wCW	3 < T < 14	18 < S < 30.8
warm Shelf Water	wSW	3 < T < 14	30.8 < S < 33.4
Modified Winter Water	MWW	−1 < T < 0	30.8 < S < 33.8
Winter Water	WW	−2 < T < −1	30.8 < S < 35
Atlantic Water & Bering Basin Water	AtlW & BBW	−1 < T < 3 3 < T < 5	34 < S < 35 33.8 < S < 35
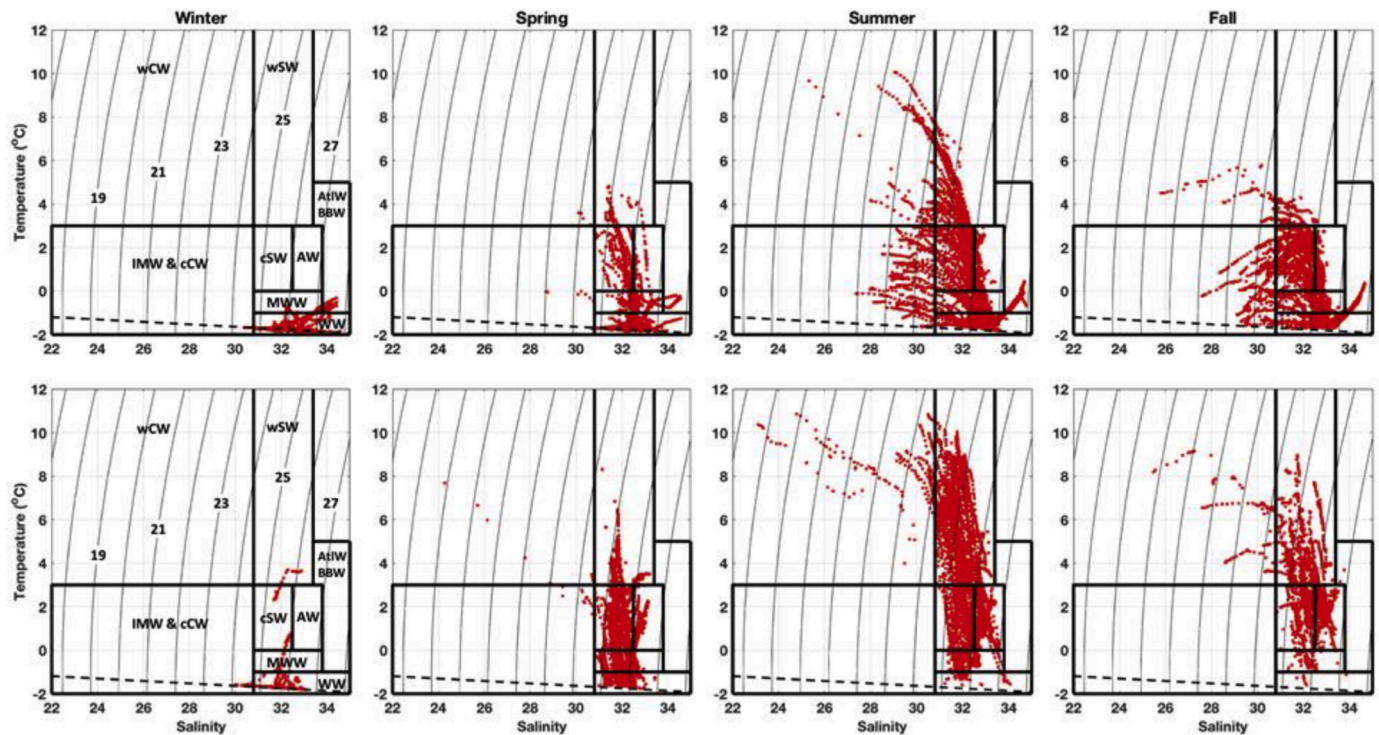
Fig. 4. Seasonal climatology T-S distributions for the Chukchi Shelf (top) and the Bering Shelf (bottom). Water masses shown in Fig. 5 are outlined by black lines and definitions are given in Table 2. The freezing point curve is marked with a dashed line. Sigma-t contours are labeled in the lower left panel. Abbreviations include wCW = warm Coastal Water; wSW = warm Shelf Water; IMW = Ice Melt Water; cCW = cool Coastal Water; cSW = cool Shelf Water; AnW = Anadyr Water; WW = Winter Water; AtlW = Atlantic Water; BBW = Bering Basin Water.

(wSW) and cool Shelf Water (cSW) designations encompass the BSW category of Coachman et al. (1975).

Winter months are the most sparsely sampled and many grid cells lack any profiles at all. For those cells containing data, most show Winter Water (WW) characteristics with temperatures close to the freezing point (T < −1 °C), although modestly elevated temperatures (−1.0 °C < T < 1.0 °C) are found at depth along the outer Bering Shelf and near the Chukchi Slope, including some waters at the edge of the Arctic basin below 150 m depth that exhibit contributions of Atlantic Water (AtlW). The southernmost few grid points in the Bering Sea have the warmest waters in winter (T > 2.0 °C), suggesting heat entering the Bering Shelf via advection up Bering Canyon from the North Aleutian Slope Current (Stabeno et al., 2009) or coming through Unimak Pass (Stabeno et al., 2002, 2017). Relatively high salinities (>32.5) are observed in or near to known dense water formation regions, including over much of the southern Chukchi Sea and near the St. Lawrence Island polynya (Danielson et al., 2006). In winter, riverine influence (CCW) is detected in Norton Sound and along the Chukchi Siberian coastline (Fig. 5). We note that cold and fresh coastal runoff is not readily distinguishable from Ice Melt Water (IMW) or the cold fresh water of the SCC in summer (Weingartner et al., 1999) using only temperature and salinity tracers but isotopic tracers can separate them readily (e.g. Cooper et al., 2005).

Spring data show that cSW is prevalent in the upper portion of the water column on both shelves due to the combined effects of seasonal warming and freshening from ice melt. IMW is found at some stations near coasts, but low salinity ice-melt plumes (e.g. S < 28) are not generally observed across the middle of either shelf in spring. The latter point suggests that ice melt (S ∼ 7) quickly mixes and is diluted by mixing with ambient shelf waters, or possibly that interannual variability in the ice extent combined with the climatology averaging obscures the ice melt signal. We detect little IMW in the Bering Sea in the climatology, but it is a dominant surface water mass across the northern and northwestern Chukchi Sea in summer and fall. The Bering Shelf

upper water column at this time of year mostly contains wSW except for low-salinity wCW of the riverine coastal domains, especially within the large river-fed embayments: the Gulf of Anadyr, Bristol Bay, Norton Sound and Kotzebue Sound. Possibly shunted offshore by winds or bathymetry, wCW is also found offshore south of St. Lawrence Island and relatively far offshore in the northeast Chukchi Sea.

Low temperature waters (<2 °C) of the Bering Sea cold pool extend from the northwest portion of the eastern Bering Shelf along the mid-shelf region (e.g. along the 70-m isobath), past the Pribilof Islands, and into the southern reaches of the southeast Bering Sea in years with extensive ice cover (Takenouti and Ohtani, 1974). The cold pool region contains near-bottom waters classified as WW or cSW through all seasons. These temperature-salinity characteristics also occupy the lower portion of the water column across much of the northern and north-eastern Chukchi Shelf in summer.

Following the main pathway of nutrient-rich currents feeding the highly productive portions of the Pacific Arctic, saline (S > 32.5) AnW can be traced from the upper Bering slope counter-clockwise around the Gulf of Anadyr, into Chirikov Basin and through Bering Strait (orange color in Fig. 5). AnW can be found close to the seafloor at many stations in the western Chukchi Sea in summer and fall months, showing that at least some of the high-nutrient AnW entering the Pacific Arctic is not strongly mixed with the lower-salinity shelf and coastal waters in the energetic Anadyr Strait, Chirikov Basin, and Bering Strait mixing zones. However, the high level of nutrients characteristic of AnW entering Bering Strait may not be retained as the AnW crosses the Chukchi Shelf because nutrient draw-down can occur from the surface to the seafloor on this shallow shelf. It should be noted that south of the Gulf of Anadyr the orange color indicates basin/slope dichothermal water (Miura et al., 2002) having temperature and salinity characteristics close to AnW. In the future, AnW should be separated from the dichothermal water by nutrient parameters. The AnW flow pathway has been modeled in many studies (Kinder et al., 1986; Overland and Roach, 1987; Clement et al.,
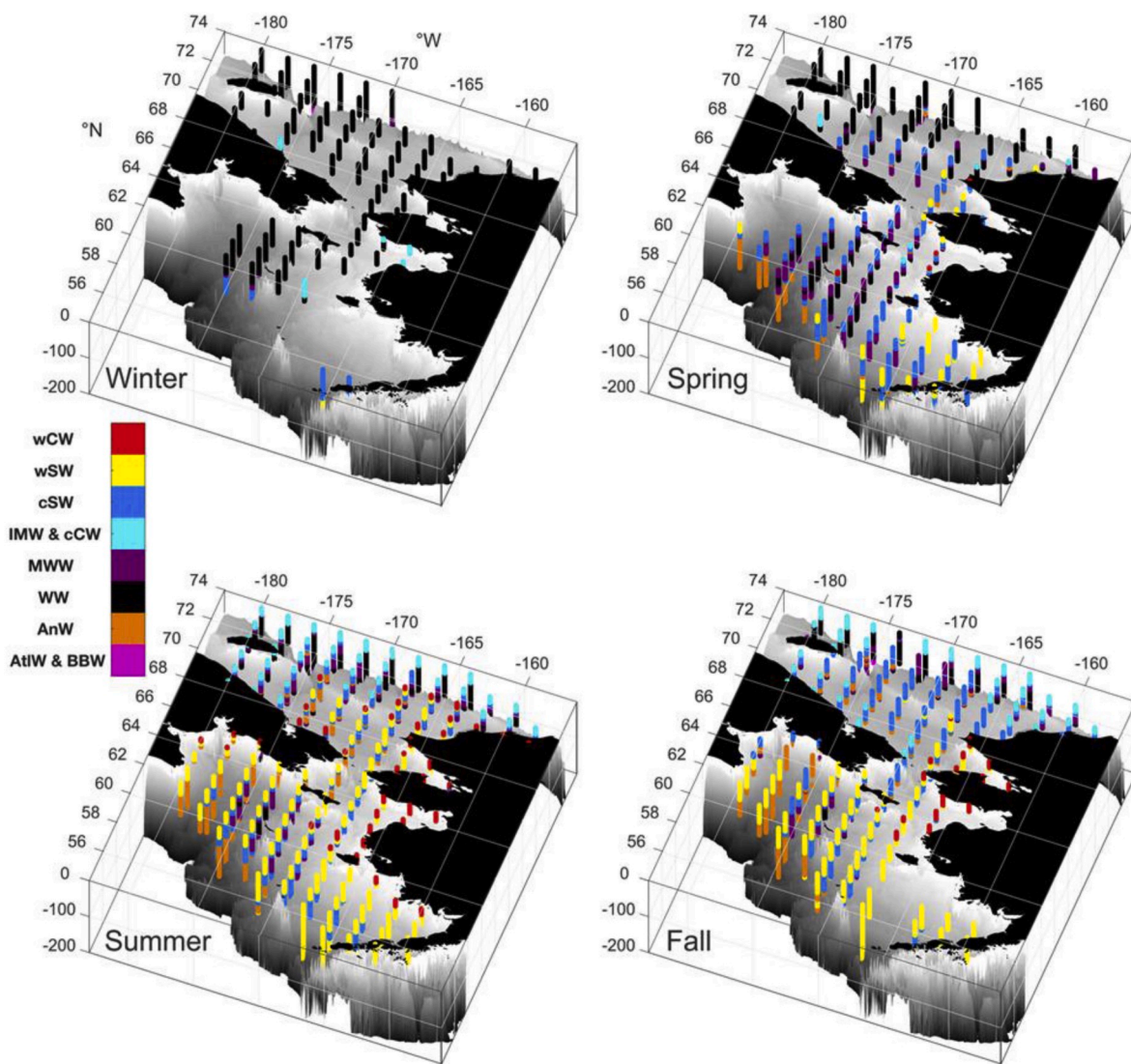
Fig. 5. Perspective view of the water seasonal climatology water mass distribution on the Bering and Chukchi shelves for winter (upper left), spring (upper right), summer (lower left) and fall (lower right) using data from before 2014. The AtlW water mass is mostly hidden behind the seafloor of the northward-facing Chukchi slope due to the perspective view. Seafloor topography (gray shading) is shown only for depths shallower than 200 m. Latitude and longitude markings are associated with the −200 depth level. Abbreviations include wCW = warm Coastal Water; wSW = warm Shelf Water; IMW = Ice Melt Water; cCW = cool Coastal Water; cSW = cool Shelf Water; AnW = Anadyr Water; WW = Winter Water; AtlW = Atlantic Water; BBW = Bering Basin Water. Note that water mass colors do not correspond to the colors of the flow field shown in Fig. 1. (For interpretation of the references to color in this figure legend, the reader is referred to the Web version of this article.)

2005; Danielson et al., 2012b, 2014) but direct observations of the Anadyr Current are few (Coachman and Shigaev, 1992; Overland et al., 1996). Our climatology supports prior diagnoses of this pathway location because the near-bottom waters flowing through Bering Strait have relatively high summer salinities (S ~ 32.5) (Woodgate, 2018), while cold pool waters and waters farther east are for the most part considerably fresher (S < 32) (Fig. S2). Hence, the fresher waters of the cold pool cannot be the source for the high-salinity component of the flow field entering Bering Strait. Although moorings (Danielson et al., 2006) and shipboard data (Grebmeier and Cooper, 1995) show the presence of a mean west-to-east current on the south side of St Lawrence Island, AnW does not appear in the climatology here, suggesting that eastward advection of AnW in the St. Lawrence Current is diluted by westward-flowing low salinity surface waters from the Alaskan coastal domain (Danielson et al., 2006, 2012a).

The seasonal evolution of the water masses on these shelves (Figs. 4 and 5) reveals a few fundamental differences between the Bering and Chukchi shelves and their adjoining slope regions. In the summer and fall, Bering Shelf WW exists in the climatology only as remnants in the

northern portion of the cold pool but can be found in significant quantities year-round in the northern Chukchi Sea. IMW is prevalent in the Chukchi Sea but nearly absent from the Bering Shelf year-round. High salinity (>34) basin waters exist at shallower depths along the upper Chukchi Slope than along the Bering Sea Slope (not shown). Our examination of the seasonal climatology provides an assessment of typical water mass characteristics and locations through the year but any individual year may look considerably different (Coachman et al., 1975). To better understand temporal variations, we turn to anomalies relative to this climatology.

3.2. Hydrography: anomalies and trends

Using our long-term climatology as a reference and motivated by our interest in placing recent conditions into the context of the prior record, we examine spatial and temporal variations of the water column hydrography. Warming is evident throughout the water column of most grid cells in the 2014–2018 average summer conditions (Fig. 6, left panel). There is less extensive sampling coverage in spring and fall, but a

similar warming is also found at most grid cells sampled in these seasons (not shown). Even in the presence of top-to-bottom warming (Fig. 6), a few locations depict a mid-depth cool anomaly, reflective of a thermocline shoaled relative to the climatology. We also observe enhanced warming in the upper water column. Strong wind-induced mixing generally resets shelf stratification with water column homogenization to a depth of at 70–100 m in winter (e.g. Kinder and Schumacher, 1981; Stabeno et al., 1998), although data from recent years suggest that the maximum depth of winter mixing may be declining (Stabeno and Bell, 2019). Lower water column properties are set annually prior to the spring onset of ice melt and surface heating that forms the characteristic two-layer Bering Shelf hydrographic structure, in which the lower water column is relatively isolated from direct atmospheric exchange (Coachman, 1986). Together, these observations suggest that the deeper warm anomalies are in place before summer stratification sets in and that heat gains through the surface during spring and summer months subsequently reinforce the surface warm anomaly.

The distribution of salinity anomalies is more complex than for temperature but they exhibit organized spatial structure (Fig. 6, right panel). We find a slight freshening (negative salinity anomaly) in the southernmost portion of the Bering Sea. A positive salinity anomaly extends from inner Bristol Bay to the outer slope in the band of latitudes from 57 to 59 °N and then continues to the northwest along the continental slope. Freshening exists from ~60 °N northward through Bering Strait and across much of the nearshore Alaskan Chukchi Sea. In contrast, farther offshore in the northeast, central, and southwest portions of the shelf, near-surface salinities are considerably higher than in the climatology. Despite somewhat sparse data in any given year, examination of monthly anomalies suggests that the seasonal mean depictions of Fig. 6 are not artifacts of the gridding or uneven sampling efforts.

Seasonally aggregated monthly standard anomalies (Fig. 7) and annually averaged monthly anomalies (Fig. 8) of temperature and salinity integrated through the water column and across each shelf reveal that the two shelves do not change in tight temporal synchrony, despite being advectively linked via Bering Strait. Each shelf forms its own set of thermohaline balances consistent with its local thermohaline inputs, sinks, and property modifications.

The Bering Shelf exhibits a record-length (1966–2018) summer freshening of -0.13 ± 0.13 (Fig. 7), which contrasts with a 1990–2018 0.08 ± 0.07 decade^{-1} salinization of the Bering Shelf (Fig. 8), a 1991–2015 increase of freshwater transport through Bering Strait (260 ± 170 km^3 decade^{-1}) (Woodgate, 2018) and a 1991–2015 decline in the Bering Strait salinity of -0.14 ± 0.10 decade^{-1} (Woodgate, 2018).

The Bering Shelf thermal anomaly is dominated by approximately decadal-scale variability of alternating warm and cold intervals (Stabeno et al., 2012). Many of the warm/cold transitions align with qualitatively similar decadal scale alternating warm and cold atmospheric conditions in the Bering Sea (Overland et al., 2012) but a full understanding of the causes of transition between the two phases is lacking. We note that from the 1990s to the present the amplitude of each successive warm interval peak has increased (Fig. 8) and that the 2014–2018 warm interval duration of five years has matched the previous warm phase duration maximum. Continued warm conditions in 2019 suggest that the warm phase will extend at least into a sixth consecutive year for the first time since the beginning of the Bering Sea hydrographic profile record.

Both shelves show indications of warming over their record length but the linear trend is only significant in the Chukchi Sea, where we compute a 1922–2018 summer season increasing temperature trend of 0.14 ± 0.07 °C decade^{-1}. This rate increased to 0.43 ± 0.35 °C decade^{-1} starting in 1990, the first year of the Bering Strait mooring deployment. Over 1991–2015 the Bering Strait mooring shows a temperature increase of 0.27 ± 0.23 °C decade^{-1} (Woodgate, 2018). During 2014–2018, each shelf shows anomalies that lie 1–2 standard deviations higher than the mean, corresponding to shelf-wide monthly average temperature anomalies of up to 3 °C. Relative to the climatology for the Chukchi, we find 2014–2018 mean monthly anomalies for spring, summer and fall of 3.2, 0.5 and 0.7 °C. In the Bering, corresponding anomalies for these three seasons are 1.3, 1.1 and 1.2 °C. The mean annual temperature anomaly over 2014–2018 for the two shelves combined is 1.2 °C. The highest observed 5-year average spring anomalies in the Bering Sea occurred in 2014–2018. On an annually aggregated basis, seven of the warmest ten Chukchi Shelf years have occurred
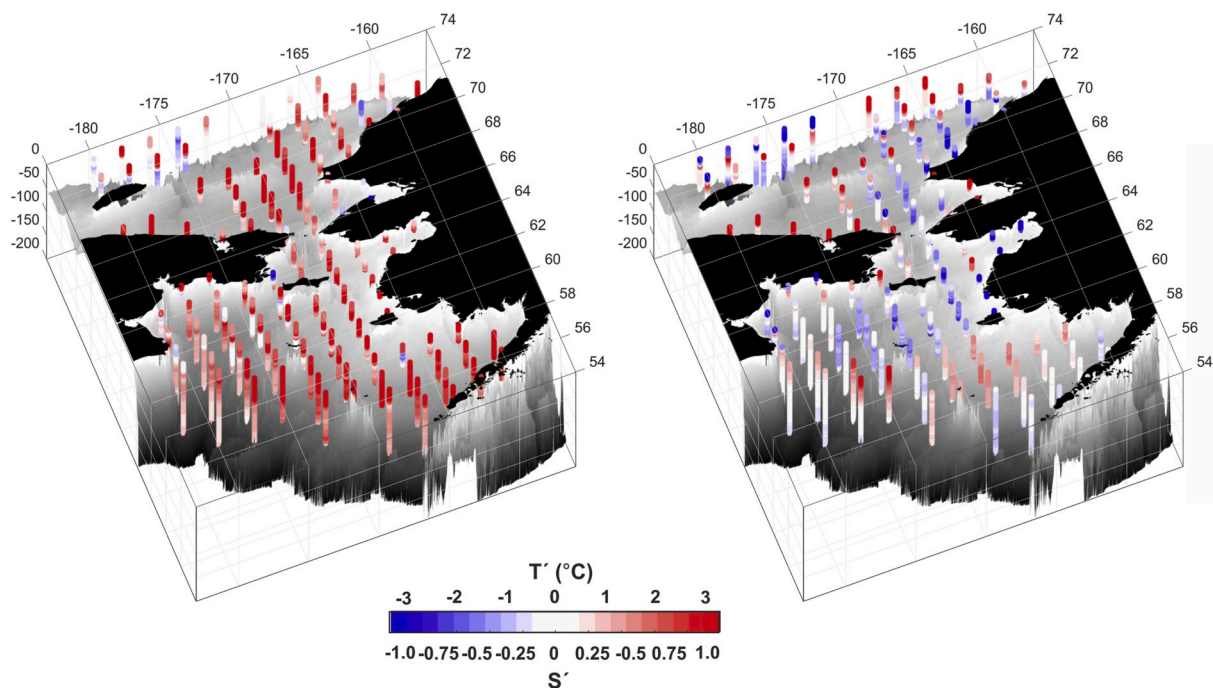

Fig. 6. Perspective view showing profiles of summer season temperature anomalies (T′; left) and salinity anomalies (S′, right) for 2014–2018 relative to data collected prior to 2014. Seafloor topography (gray shading) is shown only for depths shallower than 200 m.
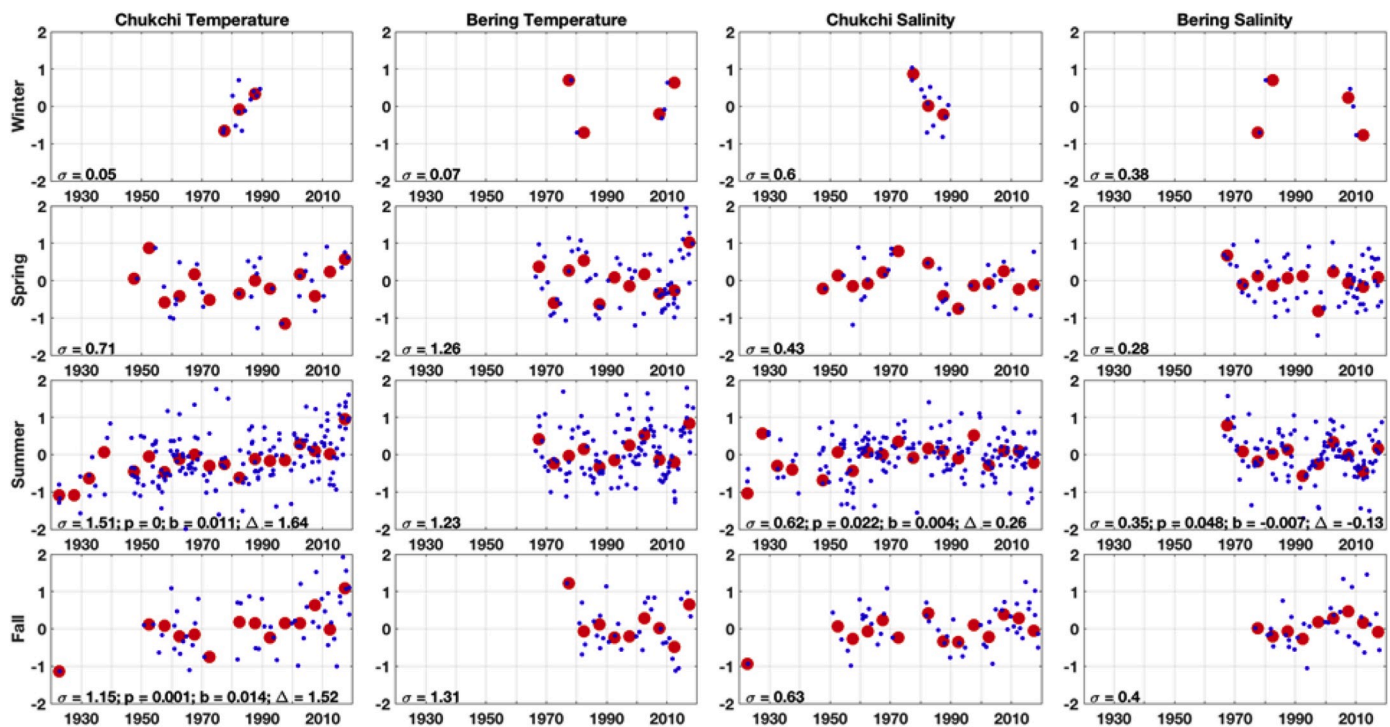
Fig. 7. Seasonally-aggregated monthly normalized temperature and salinity anomaly time series of the vertically integrated gridded profile data for the Chukchi and Bering shelves. From top to bottom, rows show seasonal aggregations for winter, spring, summer and fall, respectively. Large red dots depict 5-year averages. The standard deviation (σ) for each parameter and season is given in the lower-left corner of each panel. For records longer than 20 years that exhibit significant long-term linear trends at the 95% confidence level, the regression p-value, slope (b) and record-length change (Δ) are given. (For interpretation of the references to color in this figure legend, the reader is referred to the Web version of this article.)

since 2007 (Fig. 8), which at the time was a record-low sea-ice extent year for the Arctic as a whole (Lindsay et al., 2009). In contrast, the ten coldest anomalies are fairly evenly distributed between 1922 and 1999. We note that especially for the Chukchi Shelf, sampling is generally biased to open water areas.

There exist many more records of SST and SAT than water column profiles, so for additional context we compare our gridded temperature profile data to the gridded ERSST (Huang et al., 2017) and GISTEMP (Lenssen et al., 2019) datasets, averaging over the eastern Bering Sea, the Chukchi Shelf, the Arctic, and the globe (Fig. 8 and Supplementary Table S1). Linear trend analysis shows that all four of the integration regions and time frames have significantly increasing SST and SAT trends over each of the selected integration intervals. Over 1900–2018, the SST trend for the Bering, Chukchi, Arctic and globe are 0.10 ± 0.0, 0.08 ± 0.02, 0.05 ± 0.01, and 0.07 ± 0.01 °C decade^{-1}, respectively. Over 1990–2018, these four regions exhibit SAT trends of 0.34 ± 0.28, 0.35 ± 0.14, 0.27 ± 0.05, and 0.13 ± 0.03 °C decade^{-1}, showing that in recent decades the Pacific Arctic is warming both in the atmosphere and the ocean more quickly than the globe as a whole.

Water column thermal anomalies are correlated ($p < 0.05$) with SST variations for both shelves, with correlation coefficients of $r = 0.52$ and 0.63, respectively, for the Chukchi and Bering shelves (Fig. 8). A trend from 1922 to 2018 of an increase of 0.14 ± 0.07 °C decade^{-1} for the summer/fall water column average temperature for the Chukchi Sea (Fig. 8) is consistent with the 0.11 ± 0.02 °C decade^{-1} ERSST trend over the same period. By comparison, the Bering Sea SST trend is 0.13 ± 0.04 °C decade^{-1} over 1922–2018, lending support to the notion that the Bering Sea heat content is likely increasing significantly but that decadal scale variability obscures the long-term trend.

Anomalies of data restricted to only July through October (Fig. 9) bear close resemblance to the annually averaged anomalies shown in Fig. 8. For the three extremely warm recent years of 2015, 2017 and 2018, the mean July through October temperature anomaly of 1.80 ±

0.19 °C stands 2.26 °C higher than the average anomaly, -0.46 ± 0.24 °C, for these months in all sampled years prior to 2000. These three years are 2.86 °C higher than the average anomaly of the cold 1970s decade (-1.06 ± 0.72 °C).

To summarize, trend analyses show warming of the Chukchi Shelf over the last 96 years (Figs. 7–9), and the rate of warming has increased in recent decades. This contrasts with the decadal scale variability characteristic of the Bering Shelf, which mostly masks a likely long-term warming trend in water column average temperature over 1966–2018, although the 1922–2018 Bering Sea SST record does depict a warming trend. The Pacific Arctic is warming faster than the globe as a whole and the half-decade of 2014–2018 brought previously unobserved high temperatures to both shelves that were associated with a significantly altered sea ice regime and with this, alterations to salinity distributions (Fig. 6).

3.3. Surface heat fluxes

The shelf temperature anomalies described in Sections 3.1 and 3.2 motivate us to better understand the role of atmospheric heat fluxes in setting the temperature, salinity and sea ice anomalies described above.

The Bering and Chukchi both function as high-latitude oceanic radiators, but surface heat exchanges are not spatially or temporally uniform. For the region shown in Fig. 10a, four oceanographically distinct zones of heat loss emerge in the annual averages: the central Chukchi Shelf, the Gulf of Anadyr, the eastern Bering Sea outer shelf and slope, and the Aleutian Basin (the Bering Sea Basin). Both shelves are oceanic sources of heat to the atmosphere for six months of the year and oceanic heat sinks for about four months, gaining heat from the atmosphere in spring and summer and losing heat to the atmosphere in fall and winter. April and September are transitional months, with net cooling at higher latitudes often coincident with net warming at lower latitudes. Hence, we aggregate months into quarterly and semi-annual seasonal averages.
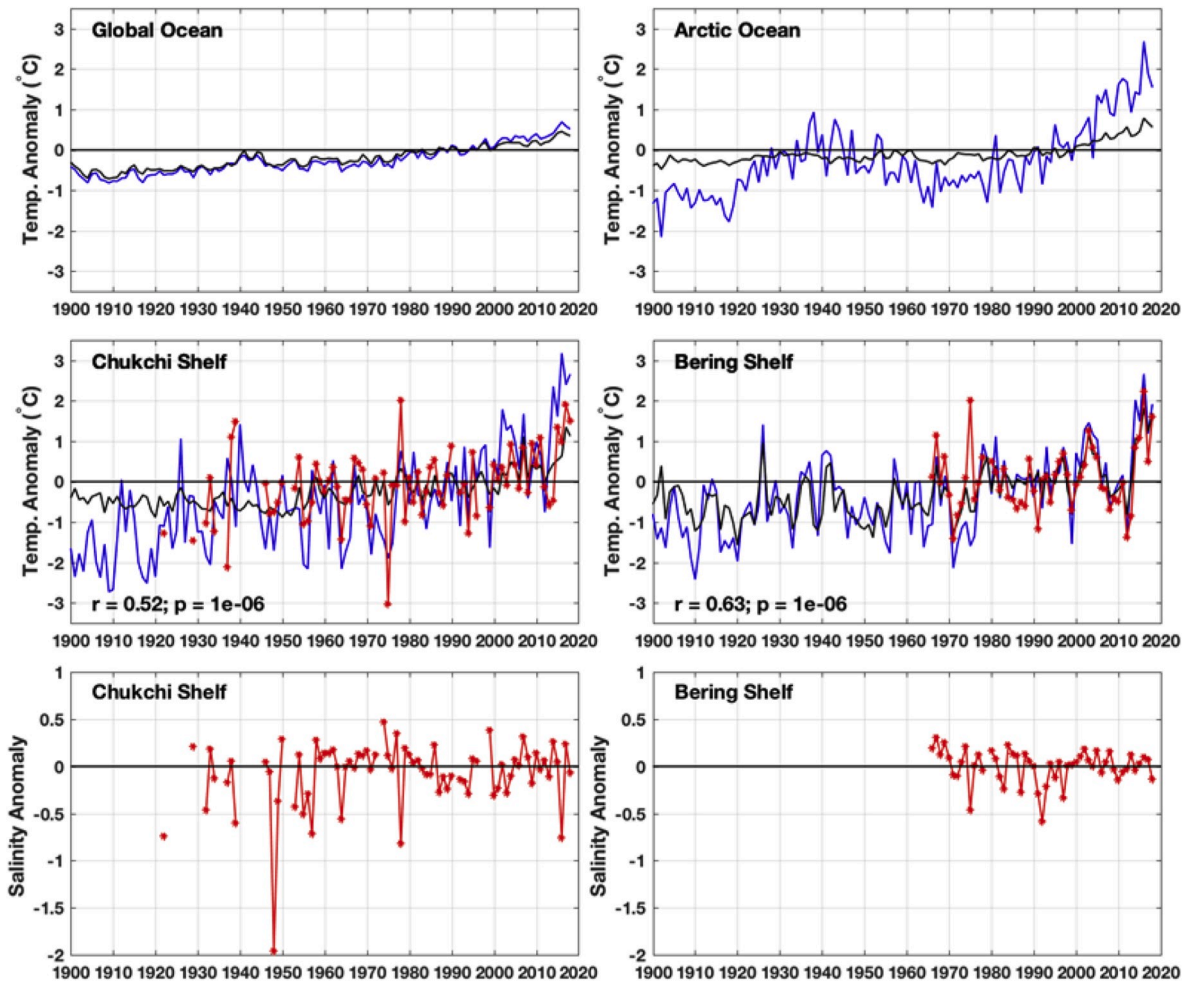
Fig. 8. Annual anomaly time series for the whole globe (upper left), the Arctic (upper right), the Chukchi Shelf (middle and lower left) and Bering Shelf (middle and lower right). Parameters include SAT (blue), SST (black), and water column temperature and salinity (both red). Correlation r and p-value statistics for the relation between the water column temperature and the SST are shown in the two middle panels. All anomalies are plotted with respect to baselines spanning the 1966–2015 half-century. (For interpretation of the references to color in this figure legend, the reader is referred to the Web version of this article.)

Comparing the climatological (1979–2013) surface heat fluxes on a quarterly basis (Table 3), we note strong seasonality in magnitude and sign and note that the Bering and Chukchi shelves have statistically different mean rates of heat exchange with the atmosphere in all seasons. Our primary focus is on the continental shelf regions but the deeper Aleutian Basin is also important to the regional heat balance so we begin there. On a per square meter basis, the Aleutian Basin is the North Pacific sub-region responsible for the greatest oceanic heat loss to the atmosphere during fall and winter months. Factors that contribute to this characteristic include the deep-water column, low winter air temperatures (Rodionov et al., 2005), energetic wind (Moore and Pickart, 2012) and tidal (Foreman et al., 2006) mixing, and the Bering Slope Current's continual advective supply of warm waters from the south (Johnson et al., 2004; Ladd, 2014). While ice is regularly advected over the northern portion of the basin and along the Kamchatka Shelf in winter, these factors keep the Aleutian Basin mostly ice-free. Open water and thin ice allow ocean-atmosphere heat exchange to occur much more readily than from a water column covered with even a few tens of centimeters of ice (Maykut, 1978; Wettlaufer, 1991; Martin et al., 2004), so Aleutian Basin waters effectively transfer available heat to the atmosphere in winter months. Despite lower air temperatures over the Chukchi through winter, the Bering Shelf loses more heat to the atmosphere in winter ($-94 \, \mathrm{W \, m^{-2}}$) than the Chukchi ($-43 \, \mathrm{W \, m^{-2}}$) because of the Bering's higher heat content at the start of fall and lower average winter ice concentrations and thicknesses. Similarly, the Bering Shelf

gains more heat from the atmosphere in spring and summer, a consequence of higher solar angle and because the Bering maintains a lower average surface albedo, so a larger fraction of the incoming shortwave radiation is absorbed.

By differencing the mean surface heat fluxes before and after 2013, we find that the northern Chukchi Shelf in the last half-decade lost appreciably more heat to the atmosphere than in years past, and the Bering Sea lost less heat (Fig. 10b and Table 3). The Chukchi Shelf increased its net cooling by ~25% (from -14 to $-18 \, \mathrm{W \, m^{-2}}$ on annual average), while the Bering Shelf remained essentially unchanged (-20 to $-18 \, \mathrm{W \, m^{-2}}$) and the Aleutian Basin lost nearly 20% of its net cooling (-27 to $-22 \, \mathrm{W \, m^{-2}}$). The potential of these changes to alter cyclogenesis, surface moisture transport, and other important meteorological processes is unclear but worthy of further investigation. The Chukchi Shelf and Aleutian Basin mean heat fluxes over 2014–2018 both lie outside of the 95% confidence interval for the mean of the 1979–2013 annual means. The changes over the two shelves do not balance, suggesting that the system is not just redistributing heat gains and losses and that net warming, cooling, and/or oceanic advective contributions must be significant. To the extent that some of the regional ocean-atmosphere heat exchange was effectively redistributed from the sub-Arctic Aleutian Basin into the Arctic Chukchi Sea, this represents a mechanism whose impact in part likely promotes reduced latitudinal gradients in air temperature.

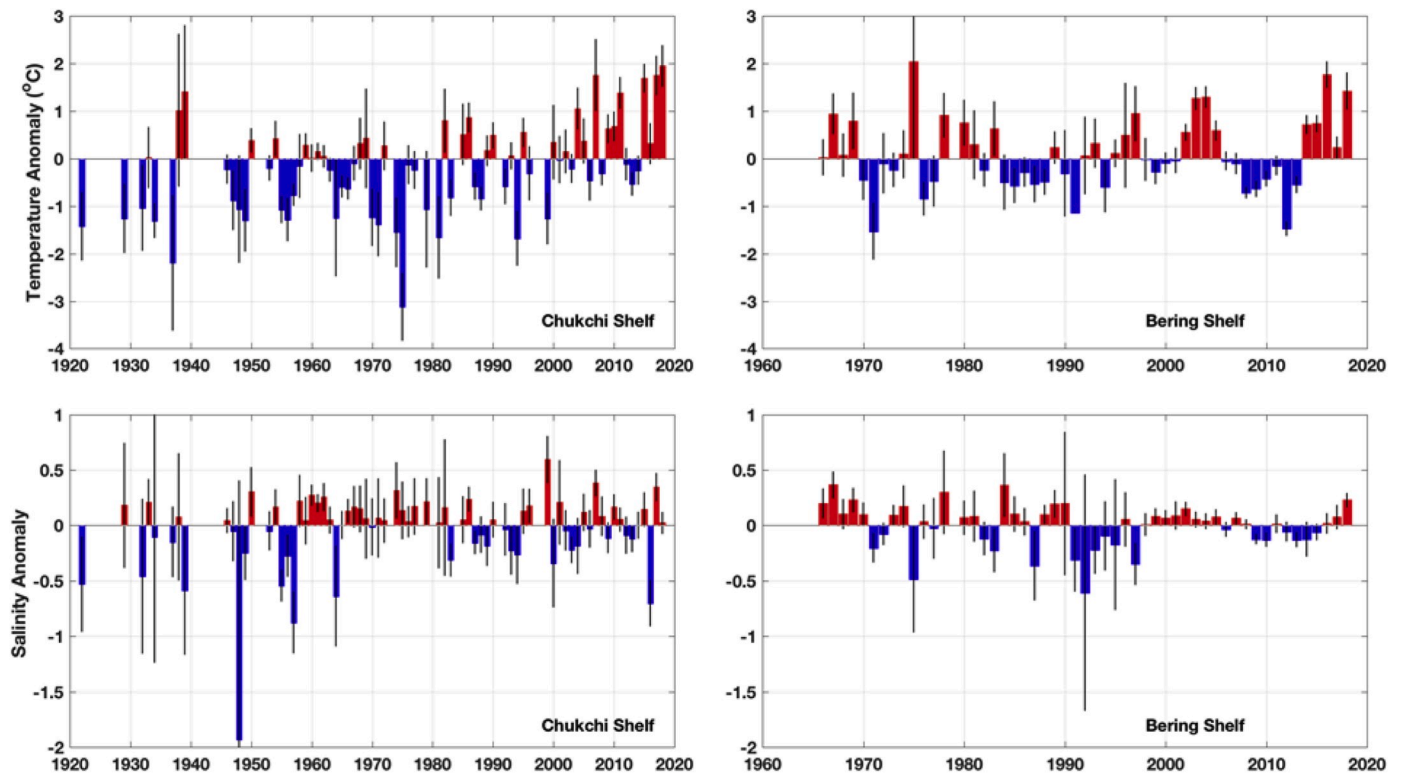Differences in the seasonal net surface heat fluxes (Fig. 11 and

Fig. 9. Annually averaged July through October thermal (top) and haline (bottom) anomalies over the Chukchi (left) and Bering (right) continental shelves. Error bar whiskers depict 95% confidence limits on the mean for each year's anomaly.
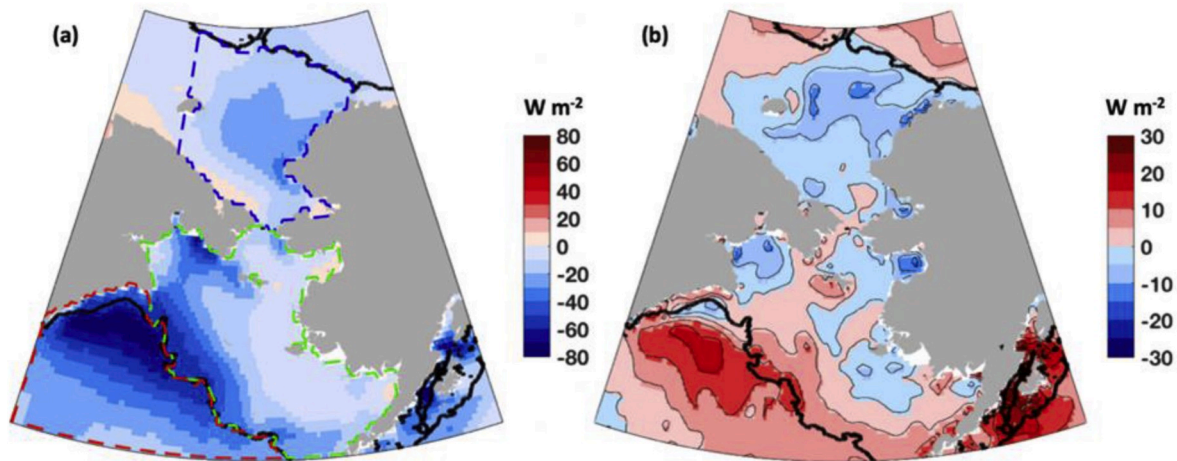

Fig. 10. (a) Mean annual surface heat flux for 1979–2013 and (b) the difference between 2014–2018 and the earlier interval, computed as the latter interval minus the earlier. Note different color bar scaling for the two panels. Edges of the continental shelves (200 m depth) are marked with a black contour. Chukchi Shelf, Bering Shelf, and Aleutian Basin integration zones discussed in the text are marked in panel (a) with blue, green and red dashed lines, respectively. (For interpretation of the references to color in this figure legend, the reader is referred to the Web version of this article.)

Table 3) for 2014–2018 relative to the climatology reveal spatial structures and temporal evolutions not apparent in the annually averaged fields, including large (often $> 5\ \mathrm{W\,m^{-2}}$) and significant changes in the mean seasonal surface heat exchanges. With the exception of summer for the Bering Shelf and Aleutian Basin, all three integration regions had 2014–2018 surface flux means that exceeded the 95% confidence limits of the 35-year climatological mean.

Over 2014–2018 the fall Chukchi heat loss increased by 30% to $-129 \pm 15\ \mathrm{W\,m^{-2}}$, a consequence of the delayed onset of ice cover and higher oceanic heat content in the fall. Given typical rates of heat loss for the ice-free ocean in fall (Table 3), a warming of about 1.3 °C for the

Bering and Chukchi shelves would require an additional month to cool the water column to the freezing point. Hence, the Chukchi Shelf now requires more time to cool to the freezing point because the shelf begins the cooling season (near the fall equinox) with a higher heat content (Section 3.2). Furthermore, the southern Bering Shelf shows a positive heat flux anomaly in the recent years that manifests in fall and winter. Diagnosis of this signal (not shown here) suggests that it is tied to decreases in the sensible and latent heat fluxes, reflecting reconfigured balances between the air-sea temperature gradient, wind speeds, and the relative humidity.

In winter, the Chukchi Shelf shows modest yet statistically significant

Table 3

Mean ERA5 net surface heat fluxes (W m^{-2}) for seasonal and year-long averaging intervals for 1979–2013 and 2014–2018 over the three integration regions denoted in Fig. 10. Limits denote 95% confidence limit on the mean for the respective interval. Positive values denote oceanic heat gain from the atmosphere; negative values are oceanic heat loss. Bold type shows when the 2014–2018 mean value lies outside of the 95% confidence interval for the 1979–2013 mean. Non-overlapping 95% confidence intervals are shown in italics.

Region	Interval	Winter JFM	Spring AMJ	Summer JAS	Fall OND	Annual Mean
Chukchi Shelf	1979–2013	*−43 ± 1*	31 ± 3	53 ± 2	−99 ± 5	−14 ± 1
	2014–2018	***−36 ± 4***	**44 ± 11**	**49 ± 8**	***−129 ± 15***	**−18 ± 4**
Bering Shelf	1979–2013	−94 ± 7	96 ± 3	67 ± 2	−146 ± 5	−19 ± 3
	2014–2018	−102 ± 15	**111 ± 7**	64 ± 7	−146 ± 11	−18 ± 6
Aleutian Basin	1979–2013	*−138 ± 7*	95 ± 2	77 ± 2	−144 ± 5	−27 ± 3
	2014–2018	*−116 ± 15*	**101 ± 6**	79 ± 2	**−154 ± 16**	**−22 ± 8**

(−43 to −36 W m^{-2}) reduction of heat loss during 2014–2018 relative to the 1979–2013 base period. Note that the Aleutian Basin loses much less heat in winter compared to previous years (−138 to −116 W m^{-2}). Examination of the individual heat flux terms for this case shows that the difference is driven primarily by anomalous sensible heat fluxes, with additional contributions from latent and longwave fluxes.

In spring, both the Bering and Chukchi shelves exhibited strong positive surface heat flux anomalies during 2014–2018, a consequence of lower ice concentrations (e.g. Fig. 2) that directly led to lower average surface albedo and greater oceanic shortwave heat absorption (see also correlations in Supplementary Tables S2–S5). In the northernmost reaches of the analysis domain (e.g. north of about 72 °N) the spring ice cover has not changed greatly, nor have the ocean-atmosphere heat fluxes changed there in the spring season.

Semi-annually aggregated surface heat flux trends over 1979–2018

show that the Bering and Chukchi shelves follow contrasting trajectories through time (Fig. 12). The Chukchi Shelf shows significant trends (p < 0.05) whereby in recent years more heat is gained in the heating season and more heat lost in the cooling season, and the cooling season standard anomaly is nearly twice larger in magnitude. These trends provide additional evidence that the Chukchi Shelf heat engine is accelerating, consistent with faster rates of transition from winter to summer ice cover conditions as identified by Danielson et al. (2017). In contrast, the Bering Shelf does not exhibit a significant trend at either time of year, in part because different portions of the Bering Shelf exhibit contrasting responses in surface heat fluxes during times of warm water and low ice, such as over 2014–2018 (see Fig. 10b).

Cross-correlations between the two shelves' seasonally averaged heat fluxes provide insights into drivers and responses. Heating season anomalies over the Chukchi Sea are correlated (r = 0.49, p = 0.001) with heating season anomalies in the Bering Sea, reflecting in part the fact that Pacific Arctic atmospheric pressure systems have typical decorrelation length scales of many hundreds or thousands of km. More importantly, surface flux anomalies of the Chukchi Sea cooling season are inversely correlated to both Chukchi (r = −0.67, p < 0.001) and Bering (r = −0.45, p = 0.003) anomalies of the prior heating season, showing that heat loss follows accumulated heat gain. In contrast, cooling season surface flux anomalies are not good predictors (p > 0.05) for the following summer season's heat flux because the freezing point provides a nearly invariant lower temperature re-set each winter.

The ERA5 reanalysis reports a 2017 October to December heat flux anomaly for the Chukchi Shelf of about 41 W m^{-2}, or nearly 200 EJ (1 EJ = 10^{18} J) integrated over three months. For a typical atmospheric heat capacity of 1 J g^{-1} °C^{-1}, this massive heat exchange would be sufficient to warm the entire Arctic troposphere by more than 1 °C. The Chukchi Shelf occupies only about 3% of the Arctic Ocean area (Table 1). This scaling shows how, through ice cover mediated feedbacks of spring heat gain and fall heat loss, the Chukchi Sea delivers an out-sized contribution to Arctic amplification. The trends of Fig. 12 show increasing frequency of large surface heat losses from the Chukchi Sea, with five of the most recent eight years exhibiting an annually averaged anomalous flux of greater than one standard deviation away
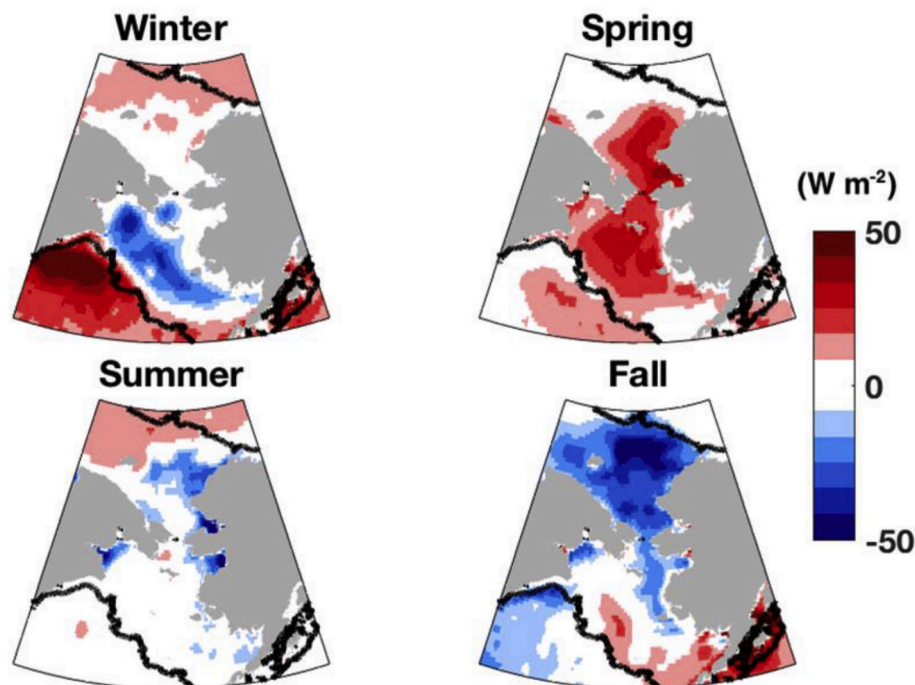
Fig. 11. Seasonal surface heat flux anomalies (W m^{-2}) for 2014–2018 relative to 1979–2013. Edges of the continental shelves (200 m depth) are marked with a black contour.
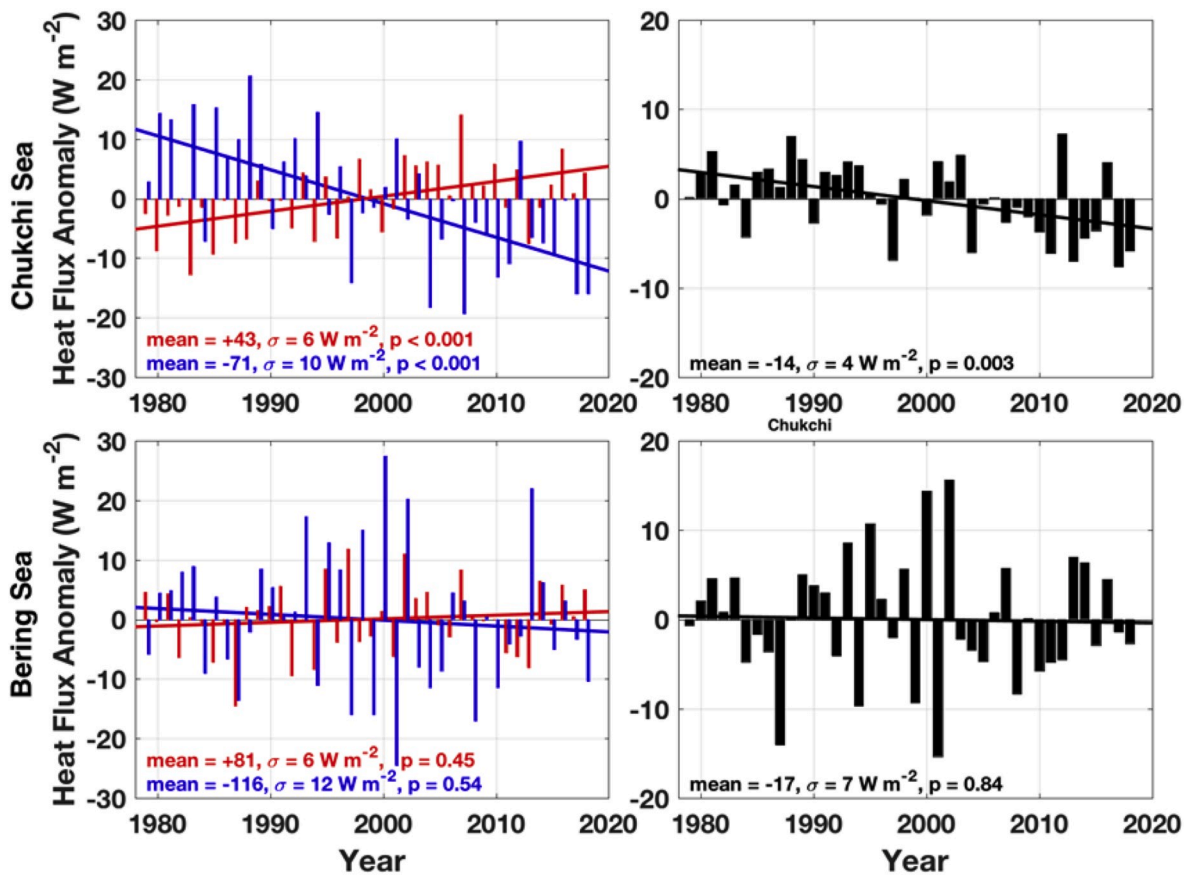
Fig. 12. Seasonally (left) and annually (right) averaged ERA5 surface heat flux anomalies for the Chukchi (top) and Bering (bottom) shelves, computed relative to a 1979–2018 record length baseline. Red bars and trend lines denote the heating spring and summer months (April–September); blue is used for the cooling fall and winter months (January–March plus October–December of the same year). Corresponding mean, standard deviations (σ) and linear trend p-values are shown at the bottom of each panel. Note different axis scales for the annual and seasonal plots. (For interpretation of the references to color in this figure legend, the reader is referred to the Web version of this article.)

from the mean (1 standard deviation = 4 W m^{-2} = 70 EJ yr^{-1} for the year).

In summary, we find statistically significant trends over the 1979–2018 period of record in the ERA5 seasonal surface heat fluxes over the Chukchi Shelf, whereby spring months are absorbing more shortwave energy, and with the lack of sea ice and a warmer ocean, fall and winter months exhibit accelerated heat losses. In contrast, the Bering Shelf does not show temporal trends in the surface heat fluxes over the last 40 years, but recent winters have lost anomalously large amounts of heat and recent spring months have absorbed more heat. The Aleutian Basin also exhibits large anomalous heat fluxes seasonally, and in recent years has delivered considerably less heat to the atmosphere than in years past. Increased heat losses to the atmosphere from the Chukchi Sea are large enough to contribute appreciably to Arctic amplification.

3.4. Bering and Chukchi Shelf heat budgets

In this section, we apply estimates of heat content, surface heat flux, and oceanic heat transport through Bering Strait to form balanced heat budgets for the Chukchi and Bering shelves. For the spring and fall, data coverage is fairly sparse so we conservatively estimate heat content changes by starting with gridded observations from 2014 to 2018 and then inserting the previously computed climatological hydrography at grid cells lacking data. Hence, heat content changes for these seasons represent a lower bound because the computation is biased toward the climatology at many grid points. We are unable to make reliable estimates for the 2014–2018 winter heat content due to lack of observations

at this time of year.

A steady state solution is obtained by integrating heat fluxes over the course of the year (Table 4 and Fig. 13). The annual integration allows us to neglect ice formation, ice melt, and the work of seasonally changing oceanic heat content because integration through one climatological (or 2014–2018 mean) calendar year exhibits zero net change in ice cover or temperature. The surface heat exchanges shown in Fig. 13 come from the annual time integrations of the ERA5 net surface heat flux shown in Table 4. The heat flux through Bering Strait is based on Bering Strait mooring A3, adjusted for instrument depths and dropouts and the mean transport in Alaskan Coastal Current transport of heat assuming a 15 m surface mixed layer (Woodgate, 2018).

The steady-state solution (Fig. 13) exhibits characteristics consistent with the heat content and surface heat flux changes described in Sections 3.1-3.3. Heat loss over the Bering Shelf exceeds that of the Chukchi by about a factor of two, primarily a consequence of the Bering Shelf's greater surface area (Table 1). The Bering Shelf is a large (~900 EJ) sink for advectively sourced heat in the North Pacific. The Chukchi Sea net surface heat flux removes from the ocean a sizeable majority (two-thirds to three-quarters) of the heat transported northward through Bering Strait.

The analysis residual represents two heat budget contributions that we cannot separate from one another: oceanic sensible heat fluxed onto or off of the shelf and the contribution of net sea ice advection - because import of sea ice to the shelves represents a potential heat sink. Lacking adequate data about changes in the sea ice flux, if we want to assess changes in sensible heat flux to the adjoining basin we are forced to assume that the advection of sea ice onto the shelf has not appreciably

Table 4

Seasonal and annual estimates of heat content and surface heat exchanges for the Bering and Chukchi continental shelves, and the northward heat flux through Bering Strait over 2014–2018, the prior period of record for each dataset, and differences between the two time periods. Annual summaries are given as net values for the fluxes and means for the heat contents. We were unable to make estimates of the winter heat content for the recent interval so conservatively assume no change.

			Winter	Spring	Summer	Fall	Annual Mean
Oceanic Heat Content (EJ)	Chukchi Shelf	1922–2013	60	130	210	200	180
		2014–2018	60	140	260	210	200
		Difference	0	10	50	10	20
	Bering Shelf	1960–2013	520	920	1200	1200	980
		2014–2018	520	1000	1500	1300	1090
		Difference	0	120	300	100	110
			Winter	**Spring**	**Summer**	**Fall**	**Annual Net**
Bering Strait Heat Advection (EJ)	Bering Strait	1990–2013	0	60	220	70	350
		2014–2016	0	80	290	100	460
		Difference	0	20	70	30	120
Ocean-Atmosphere Heat Exchange (EJ)	Chukchi Shelf	1979–2013	−180	130	240	−430	−250
		2014–2018	−160	190	220	−570	−310
		Difference	20	60	−20	−130	70
	Bering Shelf	1979–2013	−670	690	480	−1100	−560
		2014–2018	−730	800	470	−1100	−520
		Difference	−60	110	−10	0	40
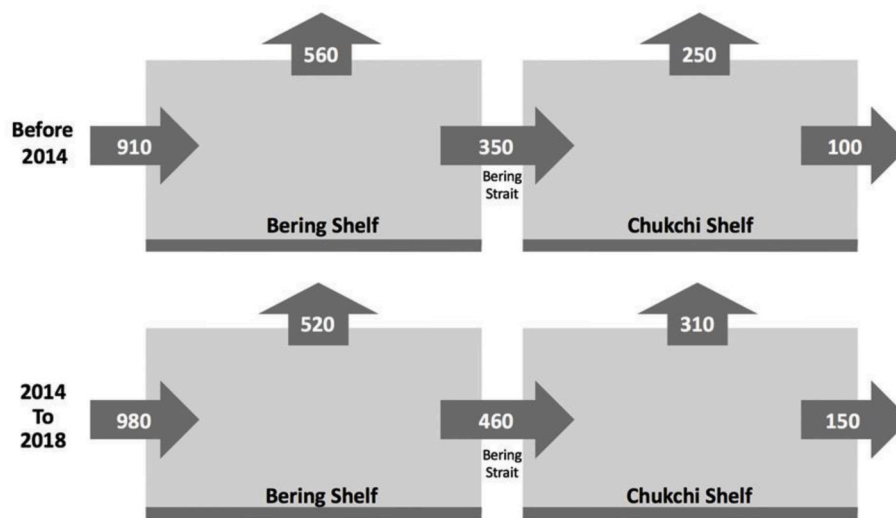
Fig. 13. Steady-state solution to the heat balance for the Bering-Chukchi Shelf system. Residual terms at the lateral shelf boundaries represent the sum of net basin-shelf sensible heat exchanges and heat budget contributions from advected sea ice. Orientation is such that the Gulf of Alaska and the Aleutian Basin are located to the left, the Canada Basin to the right and the atmosphere/ocean interface is at the top. All values reported in EJ.

changed over time. This assumption is assuredly invalid for some years so the approach has limitations but it is a useful starting point. The Chukchi Shelf annual heat budget residual is ~100 EJ, suggesting that in past decades the amount of heat fluxed off the shelf and directed into melting imported ice comprised about one quarter of the heat input northward through Bering Strait. Whether the Chukchi Shelf is a source or sink of ice varies seasonally and interannually (Howell et al., 2016) and this term is difficult to estimate. Ice can enter the Chukchi Shelf from Bering Strait (Woodgate and Aagaard, 2005), Long Strait (Weingartner et al., 1999), across the Chukchi Slope (Hutchings and Rigor, 2012) or from the Beaufort Shelf (Petty et al., 2016; Weingartner et al., 2017). In addition to the potentially significant impact of sea ice advection on the Chukchi heat budget, warm waters exiting Barrow Canyon (Itoh et al., 2015) may at times be carried back onto the Chukchi Shelf in summer and fall months, examples of which are shown with satellite tracked drifter observations by Danielson et al. (2017). Heat sourced farther offshore in the Beaufort Gyre may also be carried onto the NE Chukchi Shelf. Over the Bering Shelf, the typical ice volume near winter's end is ~1.3 × 10¹² m³ (Zhang et al., 2010), representing 400 EJ of extracted heat, or two-thirds of the Bering heat loss from summer to winter. If only 10% of the Bering ice is advected northward through Bering Strait, its

latent heat of fusion would represent a 40 EJ heat sink in the Chukchi Shelf, a relatively minor term in this shelf's heat budget, but a large fraction of the annual residual. The net export of ice through Bering Strait is estimated at ~100 km³ yr⁻¹ (Woodgate and Aagaard, 2005); we lack any good estimate of the ice transport through the other boundaries.

Relative to the earlier time interval, during 2014–2018 the Bering Strait northward heat flux increased by 30% (110 EJ), the Chukchi Shelf net (outgoing) surface heat flux increased by 25% (60 EJ) and the net heat flux residual increased by 50% (50 EJ). Simultaneously, the Bering Shelf surface heat loss diminished by 7% (40 EJ) and the advective contribution to the Bering Shelf increased (70 EJ). This advective increase represents two-thirds of the observed increase in the northward Bering Strait oceanic heat flux. Hence, the heat budget shows that the remaining 1/3 of the Bering Strait heat flux increase over 2014–2018 derives from the net decrease in the Bering Shelf surface heat exchange.

We note that the 110 EJ yr⁻¹ increase of the Bering Strait heat flux during 2014–2018 is a likely lower bound for this value because the mooring record used here misses 2017 and 2018, two of the warmest years on each shelf. Using the relation $Q = C_p * \Delta T * V * \rho * dt$ for typical annual average values of heat capacity ($C_p = 4000$ J kg⁻¹ °C⁻¹), density

($\rho = 1025$ kg m^{-3}) Bering Strait transport ($V = 1$ Sv), and from Fig. 8 the average annual temperature anomaly ($\Delta T = 1.2\,^{\circ}$C) for the two shelves over 2014–2018, we estimate a more probable Chukchi throughput increase of 150 EJ for an annual mean of 500 EJ. The impact on the annual heat budget would be an increase in the 2014–2018 Bering Shelf and Chukchi Shelf residuals to 1020 EJ yr^{-1} and 190 EJ yr^{-1}, respectively. This estimate could grow further if the Bering Strait throughflow during these years continues its increasing trend (Woodgate, 2018).

The steady state approach obscures numerous potentially important factors so we turn to a seasonally explicit solution (Fig. 14). In this analysis, we separately balance the heating season and cooling season, maintaining continuity for each season at Bering Strait. Because the seasonal heat content changes (from spring to fall and then fall to spring) are approximately equal and opposite, any change in the seasonal amplitude of shelf temperatures triggers a commensurate adjustment in the residual terms. The heat balance shows that during the cooling season the warm ocean acts as a heat source, buffering the advective supply of heat and surface heat losses. In the heating season, the large heat capacities of these expansive shelves act as heat sinks. The 2014–2018 data do not show a significant change in the spring-to-fall temperature amplitude for either shelf relative to the climatology, showing that changes in heat throughput dominate over changes in heat content. This balance also shows that oceanic and atmospheric contributions to the Chukchi Shelf heat content in the heating season are similar in magnitude, but dominated by the atmospheric contribution, and that the oceanic input over 2014–2018 increased twice as fast as the atmospheric increase.

The Bering Shelf balance suggests that the increased northward heat flux through Bering Strait comes from both increase in heat gain through the ocean surface during the heating season and increase of heat supplied via advection during the cooling season. In addition to radiating advectively sourced heat, the Bering Shelf supplies a significant amount of heat (~600 EJ) back into the Aleutian basin during the heating

season. For a 100 m winter mixed layer and the whole of the Aleutian Basin (~2×10^6 km^2), 30 EJ – the increase of Bering Shelf heat export to the basin – represents a potentially significant 0.30 $^{\circ}$C decade^{-1} Aleutian Basin upper water column warming. While removed from the Bering Shelf at least in the short term, this heat may have another opportunity to influence the Bering Shelf heat budget if it is eventually advected back onto the eastern Bering Sea shelf. In contrast, oceanic heat delivered to the Arctic through Bering Strait is lost subsequently from the Bering Sea system for many centuries.

The seasonal heat balance findings suggest that the heating season advective heat loss from the Chukchi Shelf increased by 120 EJ relative to the prior climatology. This value, more than twice the magnitude of the steady state balance increase (50 EJ), is dependent upon the magnitude of the spring-to-fall change in heat content and the influence of summer ice advection onto the Chukchi Shelf from elsewhere. Nonetheless, both heat balances describe a Chukchi Sea advective throughput that has increased appreciably. Note that Timmermans et al. (2018) document a 2014–2017 increase of heat content in the Beaufort Gyre thermocline of ~150 EJ relative to observations made over 1987–2002.

A cross-correlation analysis of the time series assembled above can provide insight into the relations between the heat fluxes, shelf temperatures and salinities, and the Bering Strait mooring data. Correlation matrices (Supplemental Tables 2–5) show the tightly interlinked nature of the various variables and the manner in which these relations evolve with the passing seasons and their adjusting heat budget balances. For example, the Chukchi ice concentration most closely co-varies with the latent heat flux in winter, the net surface heat flux in spring, and the air temperature and latent fluxes nearly equally in fall. The correlation between Chukchi latent heat flux and the ice concentration anomaly has a very high coefficient of regression in fall ($r^2 = 0.71$, $p < 0.01$) and winter ($r^2 = 0.79$, $p < 0.01$). The winter Bering ice concentration is most strongly correlated with the inverse of air temperature and shortwave
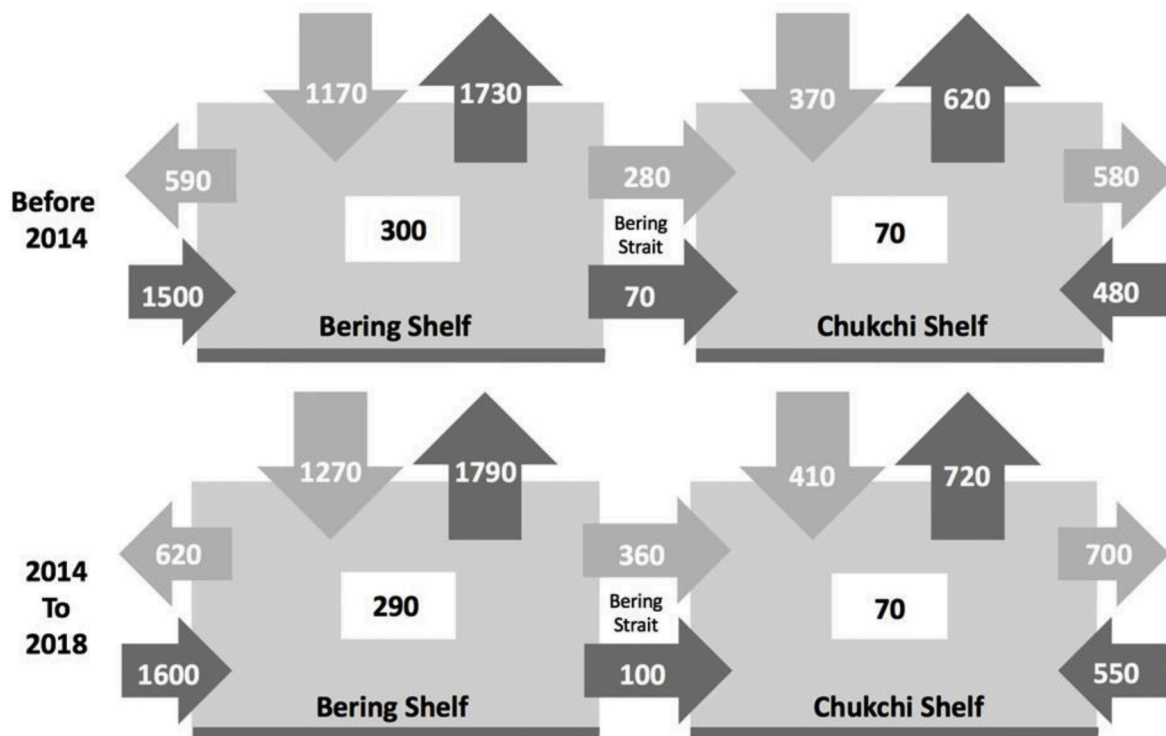

Fig. 14. Semi-annual solution of the Bering-Chukchi Shelf heat budget for the two integration intervals. Light and dark arrows denote heating and cooling season fluxes, respectively. Values in the central white boxes show the seasonal change in oceanic heat content across the heating and cooling seasons (from spring to fall and vice-versa). Figure orientation is such that the Gulf of Alaska and the Aleutian Basin are located to the left, the Canada Basin is to the right, and the atmosphere/ocean interface is at the top. All values reported in EJ.

radiation fluctuations. The Bering Sea spring ice concentration is positively correlated with the Bering Strait mooring salinity, showing that years with high ice concentrations exhibit higher salt flux to the Chukchi Sea, presumably due to enhanced brine production. The Chukchi ice concentration is negatively correlated with the Bering Strait heat flux.

Low ice anomalies in the Chukchi Sea appear to generate southerly wind anomalies (wind blowing anomalously from the south to the north) that could potentially advect ice and/or oceanic heat northward in a positive feedback relation (Tachibana et al., 2019). Thus, we examine regional wind field anomalies for 2014–2018 and correlations between monthly wind anomalies and our other variables of interest (Supplemental Tables 2–5). For the Chukchi Sea, we find that the 2014–2018 anomalous heat fluxes of winter were associated with southerly wind anomalies (Fig. 15). The net Chukchi Sea surface heat flux variations are significantly correlated ($r^2 = 0.45$, $p < 0.01$) with the meridional wind component in winter and weakly, but still significantly correlated, in fall ($r^2 = 0.08$, $p < 0.05$). The surface heat flux versus meridional wind relation in the Bering Sea is significant in both fall ($r^2 = 0.42$, $p < 0.05$) and winter ($r^2 = 0.33$, $p < 0.05$). Furthermore, the correlation analysis shows that southerly wind anomalies are significantly correlated to northward flow anomalies in Bering Strait. These findings are all consistent with the hypothesis proposed by Tachibana et al. (2019); namely, that low sea ice concentrations and excess ocean-to-atmosphere heat fluxes in the Pacific Arctic are associated with wind anomalies that also help promote reduced ice cover. Stabeno and Bell (2019) identify southerly winds in conjunction with the positive air temperature anomalies advected by these winds as key factors in driving the low ice concentrations of recent years.

In this section, we documented altered heat exchanges between these shelves, the overlying atmosphere, and the adjacent basins over 2014–2018 relative to the prior 35-year climatology. We found that the Chukchi Shelf heat engine significantly accelerated over this time, with larger heat gains in spring, larger heat content in summer in fall, and greater heat throughput to the high Arctic (110–150 EJ yr^{-1}). Anomalously high heat content of the shelves entering fall results in high oceanic heat loss to the atmosphere in fall and winter, triggering southerly wind anomalies that in turn advect warm air northward and drive water and sea ice northward.

4. Summary and discussion

Our results provide evidence for recent acceleration of the Pacific Arctic heat engine and show that the ocean plays multiple roles in the ocean-ice-atmosphere feedback loop, which are depicted schematically in Fig. 16. Relative to prior decades, the 2014–2018 heat balance is one in which the shelves absorbed more heat in the spring because of low ice concentrations and lost more heat in the fall because they begin the fall warmer and thus must lose more heat in order to reach the freezing point. Chukchi Sea surface heat fluxes trigger southerly wind anomalies that in turn promote northward advection of ice, water, and warm air, all of which lead to further reductions in winter and spring ice cover. The year-round shelf heat content has increased and the advective throughput of heat has increased. These changes are all consistent with recent observations of low ice concentrations, warm North Pacific and Pacific Arctic waters, and unusual winter storms in the northern Bering Sea. Some of these process changes were anticipated recently but have been obscured in the noise of interannual variability (see Stroeve et al. (2012) for a detailed discussion). The changes documented here help explain why the rate of warming in the Pacific Arctic has increased in recent decades, and why the Arctic is warming faster than the globe on average.

We think that some of the haline anomalies of Fig. 6, both fresh and salty, are mechanistically linked to an altered sea-ice regime, although some of the freshening is also likely due in part to the long-term decline of salinity recorded by the Bering Strait moorings (Woodgate, 2018). In the past, advection from the north carried ice southward across the Bering Sea shelf each winter and its subsequent melt at the edge of the ice pack represented a significant freshwater contribution to the shelf in water depths greater than about 70 m and especially between latitudes 56–60 °N (Zhang et al., 2010). We suggest that in recent years, the diminished southward advection effectively removed this freshwater input, resulting in the positive salinity anomalies seen near 57–59 °N. We find a typical water-column salinization of ~0.4 on the mid-shelf here (in ~70 m of water), which represents a freshwater deficit of ~0.9 m and appears reasonable relative to the expected accumulation of ~1.5 m of ice melt in a three-month winter season predicted by Zhang et al. (2010). In the northern Bering Sea and possibly the Chukchi Sea, we speculate that compounding factors likely account for the observed freshening: reduced brine production due to reduced sea-ice growth and extent (Fig. 2), and sea-ice melt along the leading (southern) ice edge
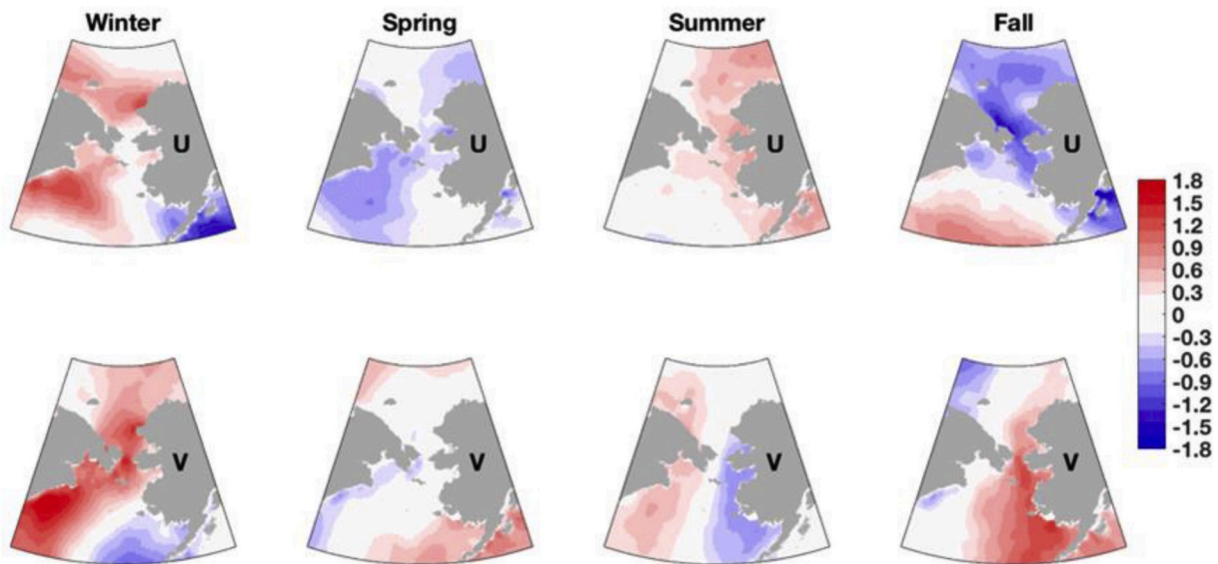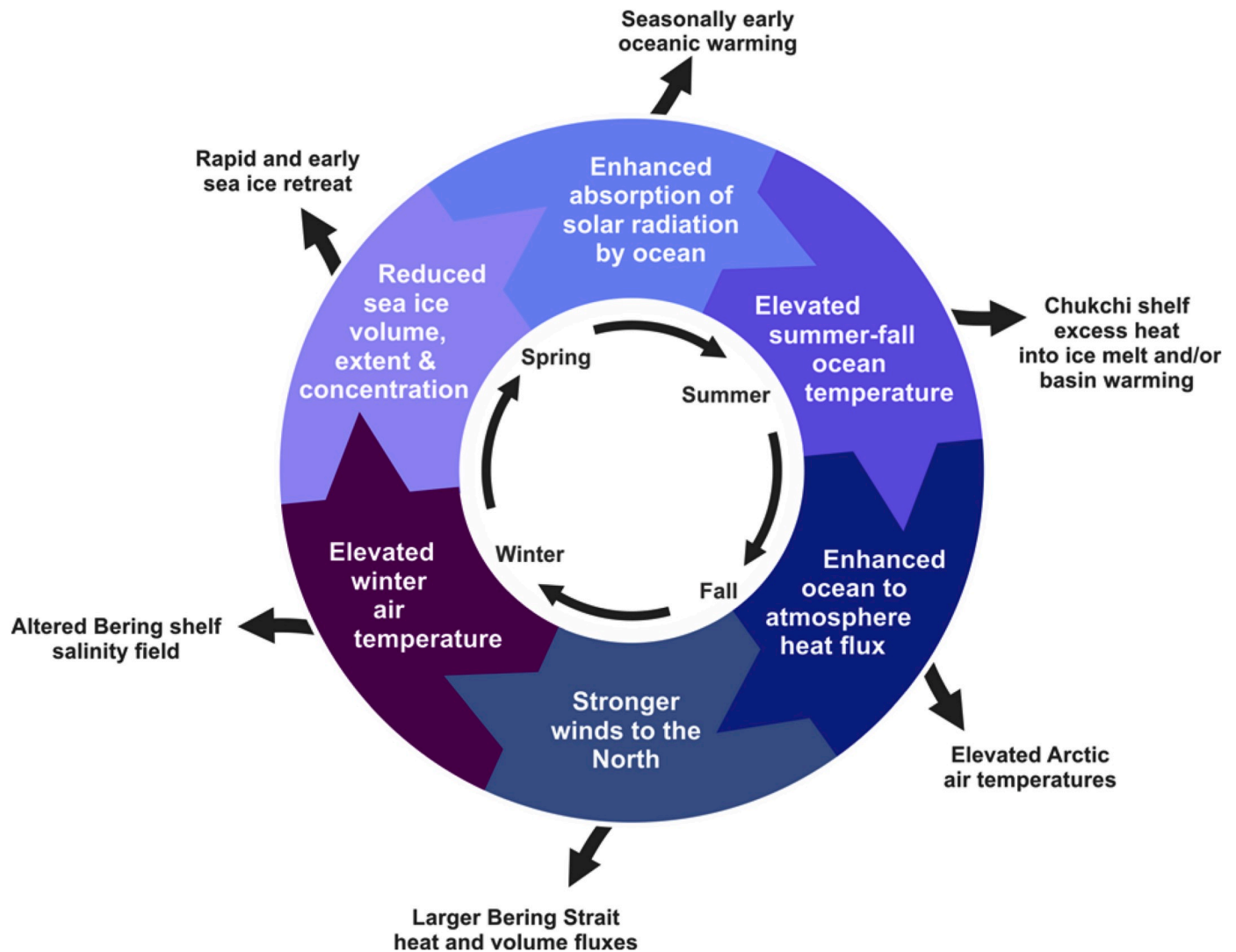

Fig. 15. Differences of seasonally averaged ERA5 wind vector components U (top row) and V (2014–2018 minus 1979–2013), units of m s-1. Note the fall and winter wind V anomalies over the Bering and Chukchi seas.

Fig. 16. The ocean-ice-atmosphere feedback loop for the Pacific Arctic's role in contributing to the Arctic amplification of air and ocean temperatures. The approximate seasonal sequence of events is shown with the inner loop (black). Physical consequences of the altered heat balances (black) include both local and remote impacts. The feedback loop promotes cascading effects on the regional physical system; not depicted here are equally important consequences for the ecosystem, for biogeochemical cycles, and for climate teleconnections that may influence weather far from the Pacific Arctic.

occurring farther north than in years past (in association with a northward-displaced freezing isotherm). Farther north, the positive salinity anomaly found near the surface in the northeast Chukchi Sea may result from at least two sources. Thinner arctic sea ice (e.g. Kwok and Rothrock, 2009; Zhang et al., 2018) would contribute less fresh water upon melting in summer. A positive saline anomaly could also develop in the ice edge plume region if the relative orientation between the winds and the ice edge is altered to promote northward ice advection. Lu et al. (2020) finds that winds from the southwest, south or east should trigger positive salinity anomalies in the meltwater plumes associated with the Chukchi marginal ice zone, so a salinization of the meltwater plume is consistent with observations of enhanced polar easterlies (e.g. Pickart et al., 2013). Further diagnosis of the sea-ice regime in relation to the shelf salinity field is clearly warranted.

Warming permafrost, outflow timing, and other hydrological changes are impacting Yukon River discharges into the Bering Sea and increasing winter season discharge rates, but annual discharge trends have not been well established for this river (Brabets and Walvoord, 2009). Since 2000, the Yukon has discharged on average 209 km^3 yr^{-1}: an increase of 3 km^3 yr^{-1}, or 1.5% above the period of record mean (Holmes et al., 2018). On the other hand, temperate glaciers around the

northern and eastern rim of the Gulf of Alaska are rapidly losing 57 ± 11 km^3 yr^{-1} of volume (Hill et al., 2015), a rate maintained since at least the early part of this century (Jacob et al., 2012; Hill et al., 2015). Long-term declines in salinity have been identified in the coastal Gulf of Alaska (Royer and Grosch, 2006) and oceanic realms of the North Pacific (Freeland, 2013). The magnitude of net glacier melt represents more than a quarter of the annual Yukon River outflow and more than 15% of all river systems that discharge onto the eastern Bering Sea shelf (Aagaard et al., 2006). Might the glacier melt in the Gulf of Alaska be partially responsible for the 2000 to present freshening observed in Bering Strait (Woodgate, 2018) and over the shelf?

We can estimate the Gulf of Alaska glaciers' potential contribution to declining Bering Shelf salinity since 2000 with the relation $S_{GF} = (S_S \cdot V_S)/(V_S + V_G)$, where S_{GF} is the shelf salinity under the influence of glacial freshening, S_S and V_S are the unfreshened shelf salinity and shelf volume, and V_G is the volume of glacial melt. Given the volume of the Bering Shelf (Table 1) and a typical shelf salinity of ~32, if only one-quarter of the Gulf of Alaska net glacial ablation were to enter the Bering Sea shelf via Unimak pass, we can account for a shelf-wide freshening of 0.015 ± 0.003 yr^{-1} (or about five times greater than the amount of freshening that the Yukon River appears to be contributing).

We conclude that the freshening signal observed in Bering Strait is at least consistent with a terrestrial discharge source from Gulf of Alaska glacial ablation.

Altered latitudinal atmospheric temperature gradients and the changing Arctic ice cover may play a role in triggering baroclinic perturbations to the atmospheric polar vortex, and with it, alterations to mid-latitude weather (Serreze and Francis, 2006; Francis and Vavrus, 2012). While a complete understanding and description of mid-to-high latitude ocean-atmosphere-climate-weather linkages is still needed, the concept is supported by theoretical considerations and evidence derived from observations, reanalysis hindcast models, and idealized process-oriented models (e.g. Holland and Bitz, 2003; Johannessen et al., 2004; Taylor et al., 2018). Very likely, when these linkages are fully resolved, our understanding will hinge on the roles played by sea ice, heat content, and heat fluxes within and between both the ocean and the atmosphere.

Tachibana et al. (2019) propose that the very presence of severely reduced ice cover over the Chukchi Shelf triggers a flow of warm southerly wind over the Bering Sea, a reinforcing feedback mechanism. Their focus was on winter, but our analysis suggests that this component of the feedback loop may be just as important in fall when the surface heat flux anomalies are the largest over the Chukchi Sea. Such feedbacks may be particularly difficult to disrupt once strongly established. As the fall warm ocean conditions become more common in a warmer world, we speculate that such winds could provide a potentially important control on the phase of polar vortex meanders (Serreze and Francis, 2006; Francis and Vavrus, 2012). If so, then improved understanding of this mechanism could lead to better predictability of atmospheric weather systems beyond the Pacific Arctic.

Only time will tell if these recent conditions represent a "new normal" as the data record shows that decadal scale variability exerts a fundamental influence. Our results suggest that to return to the pre-2014 heat balances, the cycle of low spring ice concentrations and associated low albedos must be interrupted. The heat balance suggests that such an interruption could result from advection of cooler waters onto the Bering Sea Shelf and/or winters having particularly strong and cold northerly winds. We have not determined exactly how the system entered the present state; it may have been a combination of both oceanic advection of warm waters and anomalously large surface heat fluxes.

There are physical limits to how much additional solar radiation the ocean can absorb as ice diminishes: the maximum addition available is the difference between that absorbed under current ice conditions and that reflected. As the system approaches the limit, the incoming short-wave radiation influence on the rate of change now observed in the Pacific Arctic will slow. However, continued atmospheric warming will continue to impact the oceanic heat content, latent, longwave, and sensible surface heat fluxes, and the regional heat balances. Thoman et al. (2020) find that the anomalously sparse winter sea ice conditions of 2018 will likely become the norm by the 2040s, suggesting that the 2014–2018 conditions will become increasingly common and eventually expected in any given year.

Declaration of competing interest

The authors declare that they have no known competing financial interests or personal relationships that could have appeared to influence the work reported in this paper.

CRediT authorship contribution statement

S.L. Danielson: Formal analysis, Writing - original draft, Data curation. **O. Ahkinga:** Writing - original draft, Visualization. **C. Ashjian:** Writing - original draft, Data curation. **E. Basyuk:** Writing - original draft, Data curation. **L.W. Cooper:** Writing - original draft, Data curation. **L. Eisner:** Writing - original draft, Data curation. **E. Farley:** Writing - original draft, Data curation. **K.B. Iken:** Writing - original draft, Data curation. **J.M. Grebmeier:** Writing - original draft, Data curation. **L. Juranek:** Writing - original draft, Data curation. **G. Khen:** Writing - original draft, Data curation. **S.R. Jayne:** Writing - original draft, Data curation. **T. Kikuchi:** Writing - original draft, Data curation. **C. Ladd:** Writing - original draft, Data curation. **K. Lu:** Writing - original draft, Data curation. **R.M. McCabe:** Writing - original draft, Data curation. **G.W.K. Moore:** Writing - original draft, Data curation. **S. Nishino:** Writing - original draft, Data curation. **F. Ozenna:** Writing - original draft, Visualization. **R.S. Pickart:** Writing - original draft, Data curation. **I. Polyakov:** Writing - original draft, Data curation. **P.J. Stabeno:** Writing - original draft, Data curation. **R. Thoman:** Writing - original draft, Data curation. **W.J. Williams:** Writing - original draft, Data curation. **K. Wood:** Writing - original draft, Data curation. **T.J. Weingartner:** Writing - original draft, Data curation.

Acknowledgements

number ArcticIERP-04.

Appendix A. Supplementary data

Supplementary data to this article can be found online at https://doi.org/10.1016/j.dsr2.2020.104781.

References

Aagaard, K., Coachman, L.K., Carmack, E., 1981. On the halocline of the Arctic Ocean. Deep Sea Res. Pt. A. Oceanogr. Res. Pap. 28 (6), 529–545.

Aagaard, K.A.T.R., Roach, A.T., Schumacher, J.D., 1985. On the wind-driven variability of the flow through Bering Strait. J. Geophys. Res.: Oceans 90 (C4), 7213–7221.

Aagaard, K., Weingartner, T.J., Danielson, S.L., Woodgate, R.A., Johnson, G.C., Whitledge, T.E., 2006. Some controls on flow and salinity in Bering Strait. Geophys. Res. Lett. 33 (19).

Ahlnäs, K., Garrison, G.R., 1984. Satellite and oceanographic observations of the warm coastal current in the Chukchi Sea. Arctic 244–254.

Benson, A.J., Trites, A.W., 2002. Ecological effects of regime shifts in the Bering Sea and eastern North Pacific ocean. Fish Fish. 3 (2), 95–113.

Bond, N.A., Cronin, M.F., Freeland, H., Mantua, N., 2015. Causes and impacts of the 2014 warm anomaly in the NE Pacific. Geophys. Res. Lett. 42 (9), 3414–3420.

Bourke, R.H., Paquette, R.G., 1976. Atlantic water on the Chukchi shelf. Geophys. Res. Lett. 3 (10), 629–632.

Boyer, T.P., Baranova, O.K., Coleman, C., Garcia, H.E., Grodsky, A., Locarnini, R.A., Mishonov, A.V., O'Brien, T.D., Paver, C.R., Reagan, J.R., Seidov, D., Smolyar, I.V., Weathers, K., Zweng, M.M., 2018. World Ocean Database 2018. National Centers for Environmental Information Ocean Climate Laboratory, Silver Spring, MD.

Brabets, T.P., Walvoord, M.A., 2009. Trends in streamflow in the Yukon River basin from 1944 to 2005 and the influence of the pacific decadal oscillation. J. Hydrol 371 (1–4), 108–119.

Carmack, E., Winsor, P., Williams, W., 2015. The contiguous panarctic Riverine Coastal Domain: a unifying concept. Prog. Oceanogr. 139, 13–23.

Clement, J.L., Maslowski, W., Cooper, L.W., Grebmeier, J.M., Walczowski, W., 2005. Ocean circulation and exchanges through the northern Bering Sea—1979–2001 model results. Deep Sea Res. Pt. II 52 (24–26), 3509–3540.

Coachman, L.K., 1986. Circulation, water masses, and fluxes on the southeastern Bering Sea shelf. Continent. Shelf Res. 5 (1–2), 23–108.

Coachman, L.K., Aagaard, K., 1966. On the water exchange through Bering Strait. Limnol. Oceanogr. 11 (1), 44–59.

Coachman, L.K., Shigaev, V.V., 1992. Northern bering-chukchi ecosystem: the physical basis. In: Nagel, P. (Ed.), Results of the Third Joint US-USSR Bering & Chukchi Sea Expedition (BERPAC), U.S. Fish and Wildlife Service.

Coachman, L.K., Coachman, L.K., Aagaard, K., Tripp, R.B., 1975. Bering Strait: the Regional Physical Oceanography. Univ. Washington Press.

Cooper, L.W., Benner, R., McClelland, J.W., Peterson, B.J., Holmes, R.M., Raymond, P.A., Hansell, D.A., Grebmeier, J.M., Codispoti, L.A., 2005. Linkages among runoff, dissolved organic carbon, and the stable oxygen isotope composition of seawater and other water mass indicators in the Arctic Ocean. J. Geophys. Res.: Biogeosciences 110 (G2).

Copernicus Climate Change Service (C3S), 2017. ERA5: fifth generation of ECMWF atmospheric reanalyses of the global climate. Copernicus Climate Change Service Climate Data Store (CDS). https://cds.climate.copernicus.eu/cdsapp#!/home.

Cornwall, W., 2019. Vanishing Bering Sea ice threatens one of the richest U.S. seafood sources. Science.

Coyle, K.O., Eisner, L.B., Mueter, F.J., Pinchuk, A.I., Janout, M.A., Cieciel, K.D., Farley, E. V., Andrews, A.G., 2011. Climate change in the southeastern Bering Sea: impacts on pollock stocks and implications for the oscillating control hypothesis. Fish. Oceanogr. 20 (2), 139–156.

Danielson, S., Aagaard, K., Weingartner, T., Martin, S., Winsor, P., Gawarkiewicz, G., Quadfasel, D., 2006. The St. Lawrence polynya and the Bering Shelf circulation: new observations and a model comparison. J. Geophys. Res.: Oceans 111 (C9).

Danielson, S., Weingartner, T., Aagaard, K., Zhang, J., Woodgate, R., 2012a. Circulation on the central Bering Sea shelf. J. Geophys. Res.: Oceans 117 (C10). July 2008 to July 2010.

Danielson, S., Hedstrom, K., Aagaard, K., Weingartner, T., Curchitser, E., 2012b. Wind-induced reorganization of the Bering Shelf circulation. Geophys. Res. Lett. 39 (8).

Danielson, S.L., Weingartner, T.J., Hedstrom, K.S., Aagaard, K., Woodgate, R., Curchitser, E., Stabeno, P.J., 2014. Coupled wind-forced controls of the Bering–Chukchi Shelf circulation and the Bering Strait throughflow: ekman transport, continental shelf waves, and variations of the Pacific–Arctic sea surface height gradient. Prog. Oceanogr. 125, 40–61.

Danielson, S.L., Dobbins, E.L., Jakobsson, M., Johnson, M.A., Weingartner, T.J., Williams, W.J., Zarayskaya, Y., 2015. Sounding the Northern Seas, 96. Eos.

Danielson, S.L., Eisner, L., Ladd, C., Mordy, C., Sousa, L., Weingartner, T.J., 2017. A comparison between late summer 2012 and 2013 water masses, macronutrients, and phytoplankton standing crops in the northern Bering and Chukchi Seas. Deep Sea Res. Pt. II 135, 7–26.

Dee, D.P., Uppala, S.M., Simmons, A.J., Berrisford, P., Poli, P., Kobayashi, S., Andrae, U., Balmaseda, M.A., Balsamo, G., Bauer, D.P., Bechtold, P., 2011. The ERA-Interim reanalysis: configuration and performance of the data assimilation system. Q. J. R. Meteorol. Soc. 137 (656), 553–597.

Di Lorenzo, E., Mantua, N., 2016. Multi-year persistence of the 2014/15 North Pacific marine heatwave. Nat. Clim. Change 6 (11), 1042–1047.

Doney, S.C., Ruckelshaus, M., Duffy, J.E., Barry, J.P., Chan, F., English, C.A., Galindo, H. M., Grebmeier, J.M., Hollowed, A.B., Knowlton, N., Polovina, J., 2011. Climate Change Impacts on Marine Ecosystems.

Eakins, B.W., Sharman, G.F., 2010. Volumes of the World's Oceans from ETOPO1, 7. NOAA National Geophysical Data Center, Boulder, CO.

Eppley, R.W., 1972. Temperature and phytoplankton growth in the sea. Fish. Bull. 70 (4), 1063–1085.

Foreman, M.G.G., Cummins, P.F., Cherniawsky, J.Y., Stabeno, P., 2006. Tidal energy in the Bering Sea. J. Mar. Res. 64 (6), 797–818.

Francis, J.A., Vavrus, S.J., 2012. Evidence linking Arctic amplification to extreme weather in mid-latitudes. Geophys. Res. Lett. 39 (6).

Freeland, H.J., 2013. Evidence of change in the winter mixed layer in the Northeast Pacific Ocean: a problem revisited. Atmos.-Ocean 51 (1), 126–133.

Freeman, E., Woodruff, S.D., Worley, S.J., Lubker, S.J., Kent, E.C., Angel, W.E., Berry, D. I., Brohan, P., Eastman, R., Gates, L., Gloeden, W., 2017. ICOADS Release 3.0: a major update to the historical marine climate record. Int. J. Climatol. 37 (5), 2211–2232.

Frey, K.E., Moore, G.W.K., Cooper, L.W., Grebmeier, J.M., 2015. Divergent patterns of recent sea ice cover across the bering, Chukchi, and Beaufort seas of the pacific arctic region. Prog. Oceanogr. 136, 32–49.

Gawarkiewicz, G., Haney, J.C., Caruso, M.J., 1994. Summertime synoptic variability of frontal systems in the northern Bering Sea. J. Geophys. Res.: Oceans 99 (C4), 7617–7625.

GISTEMP Team, 2019. GISS Surface Temperature Analysis (GISTEMP). NASA Goddard Institute for Space Studies. Dataset accessed 2019-07-20 at. https://data.giss.nasa.gov/gistemp/.

Gong, D., Pickart, R.S., 2016. Early summer water mass transformation in the eastern Chukchi Sea. Deep Sea Res. Pt. II 130, 43–55.

Grebmeier, J.M., Cooper, L.W., 1995. Influence of the St. Lawrence Island polynya upon the Bering Sea benthos. J. Geophys. Res.: Oceans 100 (C3), 4439–4460.

Grebmeier, J.M., Bluhm, B.A., Cooper, L.W., Danielson, S.L., Arrigo, K.R., Blanchard, A. L., Clarke, J.T., Day, R.H., Frey, K.E., Gradinger, R.R., Kędra, M., 2015. Ecosystem characteristics and processes facilitating persistent macrobenthic biomass hotspots and associated benthivory in the Pacific Arctic. Prog. Oceanogr. 136, 92–114.

Groves, D.G., Francis, J.A., 2002. Variability of the Arctic atmospheric moisture budget from TOVS satellite data. J. Geophys. Res. Atmos. 107 (D24). ACL-18.

Haiden, T., Janousek, M., Bidlot, J., Ferranti, L., Prates, F., Vitart, F., Bauer, P., Richardson, D.S., 2017. Evaluation of ECMWF Forecasts, Including 2016-2017 Upgrades (56). European Centre for Medium Range Weather Forecasts.

Hansen, J., Ruedy, R., Sato, M., Lo, K., 2010. Global surface temperature change. Rev. Geophys. 48, RG4004.

Hare, S.R., Mantua, N.J., 2000. Empirical evidence for North Pacific regime shifts in 1977 and 1989. Prog. Oceanogr. 47 (2–4), 103–145.

Hill, D.F., Bruhis, N., Calos, S.E., Arendt, A., Beamer, J., 2015. Spatial and temporal variability of freshwater discharge into the Gulf of Alaska. J. Geophys. Res.: Oceans 120 (2), 634–646.

Holland, M.M., Bitz, C.M., 2003. Polar amplification of climate change in coupled models. Clim. Dynam. 21 (3–4), 221–232.

Holmes, R.M., Shiklomanov, A.I., Suslova, A., Tretiakov, M., McClelland, J.W., Spencer, R.G.M., Tank, S.E., 2018. River discharge. In: Arctic Report Card 2018.

Howell, S.E., Brady, M., Derksen, C., Kelly, R.E., 2016. Recent changes in sea ice area flux through the Beaufort Sea during the summer. J. Geophys. Res.: Oceans 121 (4), 2659–2672.

Huang, B., Thorne, P.W., Banzon, V.F., Boyer, T., Chepurin, G., Lawrimore, J.H., Menne, M.J., Smith, T.M., Vose, R.S., Zhang, H.M., 2017. Extended reconstructed sea surface temperature, version 5 (ERSSTv5): upgrades, validations, and intercomparisons. J. Clim. 30 (20), 8179–8205.

Hunt Jr., G.L., Coyle, K.O., Eisner, L.B., Farley, E.V., Heintz, R.A., Mueter, F., Napp, J.M., Overland, J.E., Ressler, P.H., Salo, S., Stabeno, P.J., 2011. Climate impacts on eastern Bering Sea foodwebs: a synthesis of new data and an assessment of the Oscillating Control Hypothesis. ICES J. Mar. Sci. 68 (6), 1230–1243.

Hutchings, J.K., Rigor, I.G., 2012. Role of ice dynamics in anomalous ice conditions in the Beaufort Sea during 2006 and 2007. J. Geophys. Res.: Oceans 117 (C8).

Ikeda, T., 1985. Metabolic rates of epipelagic marine zooplankton as a function of body mass and temperature. Mar. Biol. 85 (1), 1–11.

Ikeda, T., Kanno, Y., Ozaki, K., Shinada, A., 2001. Metabolic rates of epipelagic marine copepods as a function of body mass and temperature. Mar. Biol. 139 (3), 587–596.

Itoh, M., Pickart, R.S., Kikuchi, T., Fukamachi, Y., Ohshima, K.I., Simizu, D., Arrigo, K.R., Vagle, S., He, J., Ashjian, C., Mathis, J.T., 2015. Water properties, heat and volume fluxes of Pacific water in Barrow Canyon during summer 2010. Deep Sea Res. Pt. I: Oceanogr. Res. Pap. 102, 43–54.

Jackson, J.M., Williams, W.J., Carmack, E.C., 2012. winter sea-ice melt in the Canada basin, Arctic Ocean. Geophys. Res. Lett. 39 (3).

Jacob, T., Wahr, J., Pfeffer, W.T., Swenson, S., 2012. Recent contributions of glaciers and ice caps to sea level rise. Nature 482 (7386), 514–518.

Johannessen, O.M., Bengtsson, L., Miles, M.W., Kuzmina, S.I., Semenov, V.A., Alekseev, G.V., Nagurnyi, A.P., Zakharov, V.F., Bobylev, L.P., Pettersson, L.H., Hasselmann, K., 2004. Arctic climate change: observed and modelled temperature and sea-ice variability. Tellus Dyn. Meteorol. Oceanogr. 56 (4), 328–341.

Johnson, G.C., Stabeno, P.J., Riser, S.C., 2004. The Bering slope current system revisited. J. Phys. Oceanogr. 34 (2), 384–398.

Kinder, T.H., Schumacher, J.D., 1981. Hydrographic Structure over the Continental Shelf of the Southeastern Bering Sea, the Eastern Bering Sea Shelf: Oceanography and

Resources, 1 DW Hood, JA Calder, 31–52. Oceanic and Atmos. Admin., Washington, DC.

Kinder, T.H., Chapman, D.C., Whitehead Jr., J.A., 1986. Westward intensification of the mean circulation on the Bering Sea shelf. J. Phys. Oceangr. 16 (7), 1217–1229.

Kwok, R., Rothrock, D.A., 2009. Decline in Arctic sea ice thickness from submarine and ICESat records: 1958–2008. Geophys. Res. Lett. 36 (15).

Kwok, R., Untersteiner, N., 2011. The thinning of Arctic sea ice. Phys. Today 64 (4), 36–41.

Ladd, C., 2014. Seasonal and interannual variability of the bering slope current. Deep Sea Res. Pt. II 109, 5–13.

Lenssen, N.J., Schmidt, G.A., Hansen, J.E., Menne, M.J., Persin, A., Ruedy, R., Zyss, D., 2019. Improvements in the GISTEMP uncertainty model. J. Geophys. Res. Atmos. 124 (12), 6307–6326.

Lin, P., Pickart, R.S., McRaven, L.T., Arrigo, K.R., Bahr, F., Lowry, K.E., Stockwell, D.A., Mordy, C.W., 2019. Water mass evolution and circulation of the northeastern Chukchi Sea in summer: implications for nutrient distributions. J. Geophys. Res.: Oceans 124 (7), 4416–4432.

Lindsay, R.W., Zhang, J., Schweiger, A., Steele, M., Stern, H., 2009. Arctic sea ice retreat in 2007 follows thinning trend. J. Clim. 22 (1), 165–176.

Lindsay, R., Wensnahan, M., Schweiger, A., Zhang, J., 2014. Evaluation of seven different atmospheric reanalysis products in the Arctic. J. Clim. 27 (7), 2588–2606.

Lu, K., Weingartner, T., Danielson, S., Winsor, P., Dobbins, E., Martini, K., Statscewich, H., 2015. Lateral mixing across ice meltwater fronts of the Chukchi Sea shelf. Geophys. Res. Lett. 42 (16), 6754–6761.

Lu, K., Danielson, S.L., Weingartner, T.J., 2020. Impacts of short-term wind events on Chukchi hydrography and sea ice retreat. Deep Sea Res. II (this volume).

Martin, S., Drucker, R., Kwok, R., Holt, B., 2004. Estimation of the thin ice thickness and heat flux for the Chukchi Sea Alaskan coast polynya from Special Sensor Microwave/ Imager data, 1990–2001. J. Geophys. Res.: Oceans 109 (C10).

Maykut, G.A., 1978. Energy exchange over young sea ice in the central Arctic. J. Geophys. Res.: Oceans 83 (C7), 3646–3658.

McPhaden, M.J., 2015. Playing hide and seek with El Niño. Nat. Clim. Change 5 (9), 791.

Miura, T., Suga, T., Hanawa, K., 2002. Winter mixed layer and formation of dichothermal water in the Bering Sea. J. oceanography 58 (6), 815–823.

Moore, G.W.K., Pickart, R.S., 2012. Northern Bering Sea tip jets. Geophys. Res. Lett. 39 (8).

Moore, S.E., Stabeno, P.J., Grebmeier, J.M., Okkonen, S.R., 2018. The Arctic Marine Pulses Model: linking annual oceanographic processes to contiguous ecological domains in the Pacific Arctic. Deep Sea Res. Pt. II 152, 8–21.

Mueter, F.J., Litzow, M.A., 2008. Sea ice retreat alters the biogeography of the Bering Sea continental shelf. Ecol. Appl. 18 (2), 309–320.

Natsuike, M., Matsuno, K., Hirawake, T., Yamaguchi, A., Nishino, S., Imai, I., 2017. Possible spreading of toxic Alexandrium tamarense blooms on the Chukchi Sea shelf with the inflow of Pacific summer water due to climatic warming. Harmful Algae 61, 80–86.

Okkonen, S., Ashjian, C., Campbell, R.G., Alatalo, P., 2019. The encoding of wind forcing into the Pacific-Arctic pressure head, Chukchi Sea ice retreat and late-summer Barrow Canyon water masses. Deep Sea Res. Pt. II 162, 22–31.

Østerhus, S., Woodgate, R., Valdimarsson, H., Turrell, B., de Steur, L., Quadfasel, D., Olsen, S.M., Moritz, M., Lee, C.M., Larsen, K.H.M., Jónsson, S., Johnson, C., Jochumsen, K., Hansen, B., Curry, B., Cunningham, S., Berx, B., 2019. Arctic Mediterranean exchanges: a consistent volume budget and trends in transports from two decades of observations. Ocean Sci. 15 (2), 379–399.

Osterkamp, T.E., Romanovsky, V.E., 1999. Evidence for warming and thawing of discontinuous permafrost in Alaska. Permafr. Periglac. Process. 10 (1), 17–37.

Overland, J.E., Roach, A.T., 1987. Northward flow in the bering and Chukchi seas. J. Geophys. Res.: Oceans 92 (C7), 7097–7105.

Overland, J.E., Wang, M., 2010. Large-scale atmospheric circulation changes are associated with the recent loss of Arctic sea ice. Tellus 62 (1), 1–9.

Overland, J.E., Stabeno, P.J., Salo, S., 1996. Direct evidence for northward flow on the northwestern Bering Sea shelf. J. Geophys. Res.: Oceans 101 (C4), 8971–8976.

Overland, J.E., Wang, M., Wood, K.R., Percival, D.B., Bond, N.A., 2012. Recent Bering Sea warm and cold events in a 95-year context. Deep Sea Res. Pt. II 65, 6–13.

Paquette, R.A., Bourke, R.H., 1974. Observations on the coastal current of Arctic Alaska. J. Mar. Res. 32 (2), 195–207.

Perovich, D.K., Richter-Menge, J.A., Jones, K.F., Light, B., 2008. Sunlight, water, and ice: extreme Arctic sea ice melt during the summer of 2007. Geophys. Res. Lett. 35 (11).

Peralta Ferriz, C., Woodgate, R.A., 2017. The dominant role of the east Siberian Sea in driving the oceanic flow through the Bering Strait—conclusions from GRACE Ocean mass satellite data and in situ mooring observations between 2002 and 2016. Geophys. Res. Lett. 44 (22), 11–472.

Petty, A.A., Hutchings, J.K., Richter-Menge, J.A., Tschudi, M.A., 2016. Sea ice circulation around the Beaufort Gyre: the changing role of wind forcing and the sea ice state. J. Geophys. Res.: Oceans 121 (5), 3278–3296.

Pickart, R.S., Moore, G.W.K., Weingartner, T.J., Danielson, S.L., Frey, K.E., 2013. Physical drivers of the Chukchi, Beaufort, and northern bering seas. Developing a Conceptual Model of the Arctic Marine Ecosystem 2.

Pickart, R.S., Nobre, C., Lin, P., Arrigo, K.R., Ashjian, C.J., Berchok, C., Cooper, L.W., Grebmeier, J.M., Hartwell, I., He, J., Itoh, M., 2019. Seasonal to mesoscale variability of water masses and atmospheric conditions in Barrow Canyon, Chukchi Sea. Deep Sea Res. Pt. II 162, 32–49.

Pisareva, M.N., Pickart, R.S., Spall, M.A., Nobre, C., Torres, D.J., Moore, G.W.K., Whitledge, T.E., 2015. Flow of pacific water in the western Chukchi sea: results from the 2009 RUSALCA expedition. Deep Sea Res. Pt. I: Oceanogr. Res. Pap. 105, 53–73.

Polyakov, I.V., Pnyushkov, A.V., Alkire, M.B., Ashik, I.M., Baumann, T.M., Carmack, E. C., Goszczko, I., Guthrie, J., Ivanov, V.V., Kanzow, T., Krishfield, R., 2017. Greater

role for atlantic inflows on sea-ice loss in the eurasian basin of the Arctic Ocean. Sci. Asia 356 (6335), 285–291.

Roach, A.T., Aagaard, K., Pease, C.H., Salo, S.A., Weingartner, T., Pavlov, V., Kulakov, M., 1995. Direct measurements of transport and water properties through the Bering Strait. J. Geophys. Res.: Oceans 100 (C9), 18443–18457.

Rodionov, S.N., Overland, J.E., Bond, N.A., 2005. The Aleutian low and winter climatic conditions in the Bering Sea. Part I: Classification. J. Clim. 18 (1), 160–177.

Royer, T.C., Grosch, C.E., 2006. Ocean warming and freshening in the northern Gulf of Alaska. Geophys. Res. Lett. 33 (16).

Screen, J.A., Simmonds, I., 2010. The central role of diminishing sea ice in recent Arctic temperature amplification. Nature 464 (7293), 1334–1337.

Serreze, M.C., Barry, R.G., 2011. Processes and impacts of Arctic amplification: a research synthesis. Global Planet. Change 77 (1–2), 85–96.

Serreze, M.C., Francis, J.A., 2006. The Arctic amplification debate. Climatic Change 76 (3–4), 241–264.

Serreze, M.C., Holland, M.M., Stroeve, J., 2007. Perspectives on the Arctic's shrinking sea-ice cover. Sci. Asia 315 (5818), 1533–1536.

Serreze, M.C., Crawford, A.D., Stroeve, J.C., Barrett, A.P., Woodgate, R.A., 2016. Variability, trends, and predictability of seasonal sea ice retreat and advance in the Chukchi Sea. J. Geophys. Res.: Oceans 121 (10), 7308–7325.

Shimada, K., Itoh, M., Nishino, S., McLaughlin, F., Carmack, E., Proshutinsky, A., 2005. Halocline structure in the Canada basin of the Arctic Ocean. Geophys. Res. Lett. 32 (3).

Stabeno, P.J., Bell, S.W., 2019. Extreme conditions in the Bering Sea (2017–2018): record-breaking low sea-ice extent. Geophys. Res. Lett. 46 (15), 8952–8959.

Stabeno, P.J., Schumacher, J.D., Davis, R.F., Napp, J.M., 1998. Under-ice observations of water column temperature, salinity and spring phytoplankton dynamics: eastern Bering Sea shelf. J. Mar. Res. 56 (1), 239–255.

Stabeno, P.J., Reed, R.K., Napp, J.M., 2002. Transport through Unimak pass, Alaska. Deep Sea Res. Pt. II 49 (26), 5919–5930.

Stabeno, P.J., Ladd, C., Reed, R.K., 2009. Observations of the aleutian north slope current, Bering Sea, 1996–2001. J. Geophys. Res.: Oceans 114 (C5).

Stabeno, P.J., Farley Jr., E.V., Kachel, N.B., Moore, S., Mordy, C.W., Napp, J.M., Overland, J.E., Pinchuk, A.I., Sigler, M.F., 2012. A comparison of the physics of the northern and southern shelves of the eastern Bering Sea and some implications for the ecosystem. Deep Sea Res. Pt. II 65, 14–30.

Stabeno, P.J., Duffy-Anderson, J.T., Eisner, L.B., Farley, E.V., Heintz, R.A., Mordy, C.W., 2017. Return of warm conditions in the southeastern Bering Sea: physics to fluorescence. PloS One 12 (9).

Steele, M., Ermold, W., Zhang, J., 2008. Arctic Ocean surface warming trends over the past 100 years. Geophys. Res. Lett. 35 (2).

Stigebrandt, A., 1984. The North Pacific: a global-scale estuary. J. Phys. Oceangr. 14 (2), 464–470.

Stocker, T.F., Qin, D., Plattner, G.K., Tignor, M., Allen, S.K., Boschung, J., Nauels, A., Xia, Y., Bex, V., Midgley, P.M., 2013. Climate Change 2013: the Physical Science Basis. Contribution of Working Group I to the Fifth Assessment Report of the Intergovernmental Panel on Climate Change, p. 1535.

Stroeve, J.C., Serreze, M.C., Fetterer, F., Arbetter, T., Meier, W., Maslanik, J., Knowles, K., 2005. Tracking the Arctic's shrinking ice cover: another extreme September minimum in 2004. Geophys. Res. Lett. 32 (4).

Stroeve, J.C., Serreze, M.C., Holland, M.M., Kay, J.E., Malanik, J., Barrett, A.P., 2012. The Arctic's rapidly shrinking sea ice cover: a research synthesis. Climatic Change 110 (3–4), 1005–1027.

Suydam, R., George, J.C., Rosa, C., Person, B., Hanns, C., Sheffield, G., Bacon, J., 2006. Subsistence Harvest of Bowhead Whales (Balaena Mysticetus) by Alaskan Eskimos during 2010. Unpubl. paper to the IWC Scientific Committee.

Tachibana, Y., Komatsu, K.K., Alexeev, V.A., Cai, L., Ando, Y., 2019. Warm hole in Pacific Arctic sea ice cover forced mid-latitude Northern Hemisphere cooling during winter 2017–18. Sci. Rep. 9 (1), 1–12.

Takenouti, A.Y., Ohtani, K., 1974. Currents and water masses in the Bering Sea: a review of Japanese work. Oceanogr. Bering Sea 2, 39–57.

Taylor, P.C., Hegyi, B.M., Boeke, R.C., Boisvert, L.N., 2018. On the increasing importance of air-sea exchanges in a thawing Arctic: a review. Atmosphere 9 (2), 41.

Thoman, R.L., Bhatt, U.S., Bieniek, P.A., Brettschneider, B.R., Brubaker, M., Danielson, S. L., Labe, Z., Lader, R., Meier, W.N., Sheffield, G., Walsh, J.E., 2020. The record low Bering Sea ice extent in 2018: context, impacts, and an assessment of the role of anthropogenic climate change. Bull. Am. Meteorol. Soc. 101 (1), S53–S58.

Timmermans, M.L., Proshutinsky, A., Golubeva, E., Jackson, J.M., Krishfield, R., McCall, M., Platov, G., Toole, J., Williams, W., Kikuchi, T., Nishino, S., 2014. Mechanisms of Pacific summer water variability in the Arctic's Central Canada Basin. J. Geophys. Res.: Oceans 119 (11), 7523–7548.

Timmermans, M.L., Toole, J., Krishfield, R., 2018. Warming of the interior Arctic Ocean linked to sea ice losses at the basin margins. Sci. Adv. 4 (8), 6773.

Tokinaga, H., Xie, S.P., Mukougawa, H., 2017. Early 20th-century Arctic warming intensified by Pacific and Atlantic multidecadal variability. Proc. Natl. Acad. Sci. Unit. States Am. 114 (24), 6227–6232.

Trenberth, K.E., Fasullo, J.T., Kiehl, J., 2009. Earth's global energy budget. Bull. Am. Meteorol. Soc. 90 (3), 311–324.

Van Vorhees, D., Lowther, A., 2010. Fisheries of the United States 2009. Current Fishery Statistics No. 2009. National Marine Fisheries Service, Silver Spring, MD, p. 103.

Walsh, J.J., McRoy, C.P., Coachman, L.K., Goering, J.J., Nihoul, J.J., Whitledge, T.E., Blackburn, T.H., Parker, P.L., Wirick, C.D., Shuert, P.G., Grebmeier, J.M., 1989. Carbon and nitrogen cycling within the Bering/Chukchi Seas: source regions for organic matter effecting AOU demands of the Arctic Ocean. Prog. Oceanogr. 22 (4), 277–359.

Walsh, J.E., Thoman, R.L., Bhatt, U.S., Bieniek, P.A., Brettschneider, B., Brubaker, M., Danielson, S., Lader, R., Fetterer, F., Holderied, K., Iken, K., 2018. The high latitude marine heat wave of 2016 and its impacts on Alaska. Bull. Am. Meteorol. Soc. 99 (1), S39–S43.

Walther, G.R., Post, E., Convey, P., Menzel, A., Parmesan, C., Beebee, T.J., Fromentin, J. M., Hoegh-Guldberg, O., Bairlein, F., 2002. Ecological responses to recent climate change. Nature 416 (6879), 389.

Weingartner, T.J., Danielson, S., Sasaki, Y., Pavlov, V., Kulakov, M., 1999. The Siberian Coastal Current: a wind-and buoyancy-forced Arctic coastal current. J. Geophys. Res.: Oceans 104 (C12), 29697–29713.

Weingartner, T.J., Danielson, S.L., Potter, R.A., Trefry, J.H., Mahoney, A., Savoie, M., Irvine, C., Sousa, L., 2017. Circulation and water properties in the landfast ice zone of the Alaskan Beaufort Sea. Continent. Shelf Res. 148, 185–198.

Weingartner, T.J., Danielson, S.L., Royer, T.C., 2005a. Freshwater variability and predictability in the Alaska coastal current. Deep Sea Res. Pt. II 52 (1–2), 169–191.

Weingartner, T., Aagaard, K., Woodgate, R., Danielson, S., Sasaki, Y., Cavalieri, D., 2005b. Circulation on the north central Chukchi Sea shelf. Deep Sea Res. Pt. II 52 (24–26), 3150–3174.

Wettlaufer, J.S., 1991. Heat flux at the ice-ocean interface. J. Geophys. Res.: Oceans 96 (C4), 7215–7236.

Wiseman Jr., W.J., Rouse Jr., L.J., 1980. A coastal jet in the Chukchi Sea. Arctic 21–29.

Woodgate, R.A., 2018. Increases in the Pacific inflow to the Arctic from 1990 to 2015, and insights into seasonal trends and driving mechanisms from year-round Bering Strait mooring data. Prog. Oceanogr. 160, 124–154.

Woodgate, R.A., Aagaard, K., 2005. Revising the Bering Strait freshwater flux into the Arctic Ocean. Geophys. Res. Lett. 32 (2).

Woodgate, R.A., Aagaard, K., Weingartner, T.J., 2005a. Monthly temperature, salinity, and transport variability of the Bering Strait through flow. Geophys. Res. Lett. 32 (4).

Woodgate, R.A., Aagaard, K., Swift, J.H., Falkner, K.K., Smethie Jr., W.M., 2005b. Pacific ventilation of the Arctic Ocean's lower halocline by upwelling and diapycnal mixing over the continental margin. Geophys. Res. Lett. 32 (18).

Woodgate, R.A., Aagaard, K., Weingartner, T.J., 2005c. A year in the physical oceanography of the Chukchi Sea: moored measurements from autumn 1990–1991. Deep Sea Res. Pt. II 52 (24–26), 3116–3149.

Woodgate, R.A., Aagaard, K., Weingartner, T.J., 2006. Interannual changes in the Bering Strait fluxes of volume, heat and freshwater between 1991 and 2004. Geophys. Res. Lett. 33 (15).

Woodgate, R.A., Weingartner, T., Lindsay, R., 2010. The 2007 Bering Strait oceanic heat flux and anomalous Arctic sea-ice retreat. Geophys. Res. Lett. 37 (1).

Woodgate, R.A., Weingartner, T.J., Lindsay, R., 2012. Observed increases in Bering Strait oceanic fluxes from the Pacific to the Arctic from 2001 to 2011 and their impacts on the Arctic Ocean water column. Geophys. Res. Lett. 39 (24).

Woodgate, R.A., Stafford, K.M., Prahl, F.G., 2015. A synthesis of year-round interdisciplinary mooring measurements in the Bering Strait (1990–2014) and the RUSALCA years (2004–2011). Oceanography 28 (3), 46–67.

Zhang, J., Woodgate, R., Moritz, R., 2010. Sea ice response to atmospheric and oceanic forcing in the Bering Sea. J. Phys. Oceangr. 40 (8), 1729–1747.

Zhang, J., Schweiger, A., Webster, M., Light, B., Steele, M., Ashjian, C., Campbell, R., Spitz, Y., 2018. Melt pond conditions on declining Arctic sea ice over 1979–2016: model development, validation, and results. J. Geophys. Res.: Oceans 123 (11), 7983–8003.